

<b>Antragstyp</b>	Schwerpunktprogramm - Einzelantrag - Neuantrag
<b>Type of Proposal</b>	Priority Programme - Individual Proposal - New Proposal
<b>Antragsdauer / Requested Duration</b>	36 Monate / 36 months
<b>Fach</b>	Strömungsmechanik
<b>Subject Area</b>	Fluid Mechanics
<b>Rahmenprojekt / Framework Project</b>	SPP 2171
<b>Titel</b>	<b>Optimierung von Mikrosäulentepichen für reversible Benetzung mithilfe gitterfreier Simulationen</b>
<b>Title</b>	<b>Optimization of micropillar carpets for reversible wetting using meshless simulations</b>
<b>Geschäftszeichen / Reference No.</b>	<b>NA 1436/3-1</b>
<b>Antragsteller / Applicant</b>	<b>Dr. Prapanch Nair</b> Friedrich-Alexander-Universität Erlangen-Nürnberg Department Chemie- und Bioingenieurwesen Lehrstuhl für Multiskalensimulation Erlangen
<b>Arbeitgeberzusage Statement by Employer</b>	Die Erklärung zur Arbeitgeberfunktion liegt noch nicht vor. A statement regarding employer status has not yet been received.

**Beantragte Mittel / Budget Request:**

	<b>Beantragt / Requested</b>		
<b>Dauer [Monate] / Duration [Months]</b>	<b>36</b>		
<b>NA 1436/3-1</b>			
<b>Summe / Total [Euro]</b>	<b>303.800</b>		
<b>Dr. Prapanch Nair</b>			
	<b>Anz. / No.</b>	<b>Dauer / Duration</b>	<b>Euro</b>
<b>Personalmittel / Funding for Staff</b>			<b>291.200</b>
Eigene Stelle 100 % / Temporary Position for Principal Investigator 100 %	1	36	209.700
Sonst. wiss. Mitarbeiterin/Sonst. wiss. Mitarbeiter 50 % / Other Research Assistant 50 %	1	36	81.500
<b>Sachmittel / Direct Project Costs</b>			<b>12.600</b>

Geräte bis 10.000 Euro, Software und Verbrauchsmaterial / Equipment up to EUR 10,000, Software and Consumables			3.000
Publikationen / Publications			3.000
Reisen / Travel			6.600

**Zusammenfassung** Die Gestaltung und Entwicklung von Mikrostrukturen mit hohem Aspektverhältnis (HAR) für hydrophobe Substrate wird bislang durch Heuristiken vorangetrieben und durch die vorliegende Lithographietechnik limitiert. Theoretisches Verständnis für das dynamische Benetzungsverhalten von HAR-Mikrostrukturen fehlt jedoch. Ein entscheidender Grund dafür ist die begrenzte optische Auflösung bei der experimentellen Beobachtungen von dynamischen Vorgängen. Daher ist der Einfluss von Biegesteifigkeit und Morphologie der HAR-Mikrostrukturen auf die Hydrophobizität sowie auf die Reversibilität des Benetzungsvorgangs nicht systematisch verstanden.

Ziel des Projekts ist die Optimierung von HAR-Mikrostruktursubstraten (auch bekannt als Mikrosäulen) unter Verwendung von dreidimensionalen gitterfreien Partikelsimulationen. Optimierungsziel ist eine erhöhte Hydrophobizität sowie die Verringerung der Hysterese. Als Designvariablen werden Dichte, Aspektverhältnis und Biegesteifigkeit der Säulen herangezogen. Die Interaktion zwischen der inkompressiblen Flüssigkeit (mit einer freien Oberfläche) und dem komplex geformten, festen Substrat wird durch eine gitterfreie Diskretisierung des Kontinuums simuliert. Die Kapillarkräfte werden simuliert, indem das Kontinuum mit paarweise interpartikulären Kräften überlagert wird. Mit diesen Simulationen können quantitative Beziehungen zwischen den mechanischen Eigenschaften der Mikrostruktur und den dynamischen Kontaktwinkeln hergestellt werden. Darüber hinaus beabsichtigen wir optimale HAR-Mikrostrukturdesigns für verschiedene Benetzungsregime vorzuschlagen. Als Teil eines Schwerpunktprogramms hat dieses Projekt den Vorteil, dass die Simulationen gegen experimentell hergestellte Oberflächen getestet und validiert werden können. Darüber hinaus unterstützt die Kollaboration mit Experimentatoren bei der Berücksichtigung von Fertigungseinschränkungen, so dass die, in der Simulation untersuchten Systeme, so realistisch wie möglich gehalten werden können.

Das Projekt beinhaltet drei Bearbeitungsschwerpunkte. Der erste Schwerpunkt umfasst eine Reihe von Validierungsfällen, bei denen zwei- und dreidimensionale Tropfen auf starren HAR-Mikrostrukturen mit Theorie und Experiment verglichen werden. In diese Studien wird auch die Auswirkung von Viskosität und Trägheit auf den scheinbaren Kontaktwinkel differenziert betrachtet. Im zweiten Schwerpunkt wird die Biegesteifigkeit als Parameter zur Identifizierung unterschiedlicher Benetzungsregime eingeführt. Der dritte Schwerpunkt wird zudem die Aggregation der Mikrosäulen während der Tropfenbewegung sowie die Tropfenverdampfung untersuchen.

**Summary** The design and development of high aspect ratio (HAR) microstructures for hydrophobic substrates are driven by heuristics and limited to the lithography technique at hand. Theoretical understanding of the dynamic wetting of HAR microstructures is lacking, primarily due to limitations in the resolution of experimental observations in dynamic scenarios. Therefore the role of flexural stiffness and morphology of the HAR microstructures on hydrophobicity and wetting reversibility is not fully understood.

The project aims at optimizing HAR microstructure (also known as micropillar) substrates, using three dimensional particle based meshless simulations. The goals of the optimization are increased hydrophobicity and

reduced hysteresis with the pillar density, aspect ratio of pillars and flexural strength of the substrate material as the parameters. Incompressible single component fluid (with a free surface) interacting with deformable, complex shaped solid substrates will be simulated by meshless discretization of the continuum description. The capillary forces will be simulated by superimposing pairwise inter-particle forces on the continuum domain. The simulations will provide quantitative relationships between microstructure mechanical properties and the dynamic contact angles. Further, we aim to propose optimal HAR microstructure designs for different wetting regimes. As part of a priority program this project has the advantage of testing and validating the simulations against fabricated experimental surfaces. Also, the collaborations with experimental research groups would serve as a guide to keep the simulations as realistic as possible.

The project aims at three groups of deliverables. The first is a set of validations of two and three dimensional drops on rigid HAR microstructures against theory and experiments. This group of studies would also differentiate between the effect of viscosity and inertia on the apparent contact angle. The second group of deliverables will introduce flexural stiffness as a parameter to identify different wetting regimes. The third group of deliverables will investigate micropillar aggregation during drop motion as well as drop evaporation.

# **Abstract**

The design and development of high aspect ratio (HAR) microstructures for hydrophobic substrates are driven by heuristics and limited to the lithography technique at hand. Theoretical understanding of the dynamic wetting of HAR microstructures is lacking, primarily due to limitations in the resolution of experimental observations in dynamic scenarios. Therefore the role of flexural stiffness and morphology of the HAR microstructures on hydrophobicity and wetting reversibility is not fully understood.

The project aims at optimizing HAR microstructure (also known as micropillar) substrates, using three dimensional particle based meshless simulations. The goals of the optimization are increased hydrophobicity and reduced hysteresis with the pillar density, aspect ratio of pillars and flexural strength of the substrate material as the parameters. Incompressible single component fluid (with a free surface) interacting with deformable, complex shaped solid substrates will be simulated by meshless discretization of the continuum description. The capillary forces will be simulated by superimposing pairwise inter-particle forces on the continuum domain. The simulations will provide quantitative relationships between microstructure mechanical properties and the dynamic contact angles. Further, we aim to propose optimal HAR microstructure designs for different wetting regimes. As part of a priority program this project has the advantage of testing and validating the simulations against fabricated experimental surfaces. Also, the collaborations with experimental research groups would serve as a guide to keep the simulations as realistic as possible. The project aims at three groups of deliverables. The first is a set of validations of two and three dimensional drops on rigid HAR microstructures against theory and experiments. This group of studies would also differentiate between the effect of viscosity and inertia on the apparent contact angle. The second group of deliverables will introduce flexural stiffness as a parameter to identify different wetting regimes. The third group of deliverables will investigate micropillar aggregation during drop motion as well as drop evaporation.

# **Zusammenfassung**

Die Gestaltung und Entwicklung von Mikrostrukturen mit hohem Aspektverhrltnis (HAR) fr hydrophobe Substrate wird bislang durch Heuristiken vorangetrieben und durch die vorliegende Lithographietechnik limitiert. Theoretisches Verstndnis fr das dynamische Benetzungsverhalten von HAR-Mikrostrukturen fehlt jedoch. Ein entscheidender Grund dafr ist die begrenzte optische Auflsung bei der experimentellen Beobachtungen von dynamischen Vorgngnen. Daher ist der Einfluss von Biegesteifigkeit und Morphologie der HAR-Mikrostrukturen auf die Hydrophobizitt sowie auf die Reversibilitt des Benetzungsvorgangs nicht systematisch verstanden.

Ziel des Projekts ist die Optimierung von HAR-Mikrostruktursubstraten (auch bekannt als Mikrosulen) unter Verwendung von dreidimensionalen gitterfreien Partikelsimulationen. Optimierungsziel ist eine erhhte Hydrophobizitt sowie die Verringerung der Hysterese. Als Designvariablen werden Dichte, Aspektverhrltnis und Biegesteifigkeit der Sulen herangezogen. Die Interaktion zwischen der inkompressiblen Flssigkeit (mit einer freien Oberflche) und dem komplex geformten, festen Substrat wird durch eine

gitterfreie Diskretisierung des Kontinuums simuliert. Die Kapillarkräfte werden simuliert, indem das Kontinuum mit paarweise interpartikulären Kräften belagert wird. Mit diesen Simulationen können quantitative Beziehungen zwischen den mechanischen Eigenschaften der Mikrostruktur und den dynamischen Kontaktwinkeln hergestellt werden. Darüber hinaus beabsichtigen wir optimale HAR-Mikrostrukturdesigns für verschiedene Benetzungsregime vorzuschlagen. Als Teil eines Schwerpunktprogramms hat dieses Projekt den Vorteil, dass die Simulationen gegen experimentell hergestellte Oberflächen getestet und validiert werden können. Darüber hinaus unterstützt die Kollaboration mit Experimentatoren bei der Berücksichtigung von Fertigungseinschränkungen, so dass die, in der Simulation untersuchten Systeme, so realistisch wie möglich gehalten werden können.

Das Projekt beinhaltet drei Bearbeitungsschwerpunkte. Der erste Schwerpunkt umfasst eine Reihe von Validierungsfällen, bei denen zwei- und dreidimensionale Tropfen auf starren HAR-Mikrostrukturen mit Theorie und Experiment verglichen werden. In diese Studien wird auch die Auswirkung von Viskosität und Trägheit auf den scheinbaren Kontaktwinkel differenziert betrachtet. Im zweiten Schwerpunkt wird die Biegesteifigkeit als Parameter zur Identifizierung unterschiedlicher Benetzungsregime eingeführt. Der dritte Schwerpunkt wird zudem die Aggregation der Mikrosulen während der Tropfenbewegung sowie die Tropfenverdampfung untersuchen.

# Project Description

Dr. Prapanch Nair

Friedrich-Alexander Universität  
Erlangen-Nürnberg (FAU)

## Optimization of micropillar carpets for reversible wetting using meshless simulations

---

### 1 State of the art and preliminary work

#### State of the art

##### a) High aspect ratio (HAR) microstructure

Two decades have passed since the discovery of the self cleaning mechanism of the leaves of a variety of plants [35]. The self cleaning happens essentially due to small area fraction of the substrate coming in contact with the liquid which also results in increased hydrophobicity and reduced resistance to the motion of the droplet, so that the droplet can pick up dust particles easily as it moves. Since then, biomimetic interests and nano fabrication advancements have resulted in innovative superhydrophobic substrates [7], specifically HAR microstructures also called micropillar carpets [18]. Several experiments have shown that the dynamic contact angle and reduced hysteresis are complex functions of the geometry of pillars, the chemical heterogeneity of their surfaces and the mechanical strength of the material [7, 15, 18]. However, all these studies have been heuristic studies based on the lithography technique available at their disposal. There has been no theoretical study to identify optimal combination of topology and material strength of micropillar substrates.

After seven decades since it was introduced, Cassie's [38] expression for the contact angle  $\theta_C$  of a drop resting at equilibrium on a chemically heterogeneous substrate with species  $i$  of area fraction  $\phi_i$  and corresponding contact angle  $\theta_i$  remains the most general theory:

$$\cos \theta_C = \sigma_i \phi_i \cos \theta_i \quad (1)$$

For a liquid drop in Cassie state (where the roughness features of the substrate are not immersed in the drop) on a rough solid substrate, this equation takes the form [27]:

$$\cos \theta_R = r\phi \cos \theta_Y + \phi - 1 \quad (2)$$

where  $\theta_R$  is the contact angle with the rough surface,  $r$  refers to the degree of roughness of the solid surface and  $\theta_Y$  is the Young's equilibrium contact angle assuming a smooth plane surface. When droplet dynamics are considered, Eq. 2 fails to predict the difference between the contact angles at the advancing and receding edges of the

droplet. This phenomenon, also known as contact angle hysteresis, is the source of resistance to the drop's motion on the surface. For self cleaning and other droplet based microfluidics applications it is desired to have a high contact angle with reduced hysteresis. Modified CB models exist in literature [20, 21, 36] which predict the receding angle, as the receding contact angle has larger room for variation as opposed to the advancing contact angle [9]. Most of these models match their own experimental results often considering only the features of the roughness at a cross section, neglecting the three dimensional distribution of roughness (or gratings) on the substrate. A theory that directly compares to experimental observations is therefore highly sought after [9]. Due to the complexities in describing microstructure morphology, chemical heterogeneity and the dynamics and flow regime of the drop, it seems sensible that different theoretical studies be performed for different regimes categorized by the solid area fraction.

### **b) High aspect ratio (HAR) microstructure**

High aspect ratio (HAR) microstructures represent a subset where the surface area ratio of the liquid–solid contact is very small. Their properties, such as large mechanical compliance, large surface area, and topography that separates the underlying substrate have allowed the design and exploration of biomimetic reversible dry adhesives [25], dynamically tuned superhydrophobic wetting surfaces [30, 32] , mechanical sensors, efficient heat transfer [23] and substrates for cell mechanics [18, 33]. The elasticity and high aspect ratio of the fibers allow deformation under capillary forces. The flexibility of the fibre and its resistance to bending are crucial parameters that contribute to dynamic wetting. Moreover flexible HAR microstructure would enter complex regimes such as self-assembly regimes where the fibers crowd together (a visual analogy would be wet fur of dogs), further affecting the wetting characteristics. Attempts to understand these systems have mostly focused on wetting of rigid fibres [16, 19, 37] or on elasto-capillary effects in planar geometries [28]. Very few studies couple these two aspects in their models. For example, an analytical model was introduced to predict the critical volume of a drop for its spreading on a flexible fibrous substrates [15]. Another study [7] shows a remarkable reduction in hysteresis when the fibres are in a buckled state. Figure 1 shows the variation of the contact angle and the maximum drop volume that remains pinned to the substrate during its tilting as a function of the aspect ratio of the fibers. These graphs suggests that micromechanics behind wetting of flexible HAR fibers is extremely complex with several wetting regimes.

### **c) Experimental and numerical approaches**

Experiments are limited by resolution on the one hand. For example, the measurement of contact angle from a sessile drop much smaller than the capillary length scale ( $\sqrt{\gamma/(\rho g)}$ , where  $\gamma$  is the surface tension,  $\rho$  is the density of the liquid and  $g$  is the acceleration due to gravity ) is difficult due to the fact that a drop touches the substrate of finite area due to the influence of gravity [24]. On the other hand, fabrication of different microstructures through a large parameter space in terms of fibre number density, flexural modulus and aspect ratio is expensive, time consuming, and in some cases, impossible. However optimal parameter combinations are important to motivate economically viable fabrications.

Numerical simulations could be extremely important to simulate wetting phenomena at the microscale to understand the interplay of flow regime, capillarity and the flexibil-

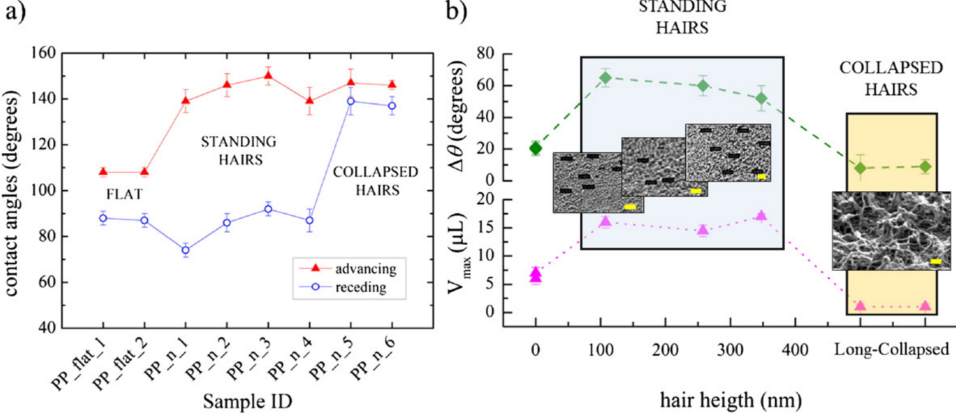


Figure 1: Variation of wetting parameters with aspect ratio (AR) of pillars in a micropillar substrate of two different materials, polypropylene and h-PDMS studied by [7]. Plot on the left shows increased hydrophobicity and reduced hysteresis as the AR increases. Even better hydrophobicity is observed when the pillars collapse due to buckling. The image on the right shows the decrease of hysteresis and the decrease in the minimum volume of the droplet required for it to roll during tilting [7].

ity of the microstructure. However, traditional computational fluid dynamics (CFD) tools such as the finite volume method (FVM) and finite difference method (FDM) suffer from severe difficulties to simulate such systems. The two major class of methods for simulating multiphase flows with capillary forces, namely, sharp interface [34] and diffuse interface [5] methods have their set of difficulties each. The former requires the contact angle to be an input parameter [22]. This does not distinguish between apparent and actual contact angles and uses ad hoc fixes to rectify the singularity that arises due to the non-slip wall boundary condition at the three phase contact line (TCL). Moreover simulating high density ratio similar to that of air-water systems require additional treatments [17]. The diffused interface methods which typically solves an equation for chemical potential (for example, the Cahn-Hilliard equation) [29] can handle heterogeneity of the substrates. But these methods are limited by the low density ratios that are achievable.

#### d) Smoothed particle hydrodynamics

Meshless methods such as smoothed particle hydrodynamics (SPH) method have the advantage of implicit mass conservation and interface tracking as a separate equation does not need to be solved for the position of the interface [31]. Though SPH is a discretization of continuum equations, it can be easily shown that the same equations of SPH can be obtained by a coarse-graining process from the molecular system. Hence SPH allows for seamless coupling between a coarse grained model and a continuum model. In fact, smoothed dissipative particle dynamics (SDPD) is one such method which is used for multiscale simulations [13].

The molecular interactions between particles can also be introduced in SPH in the context of capillary forces [6], owing to the molecular origin of surface tension [12]. In a recent publication we have shown how such molecular-like pairwise forces could be used in a way that does not interfere with the continuum viscosity formulation [2].

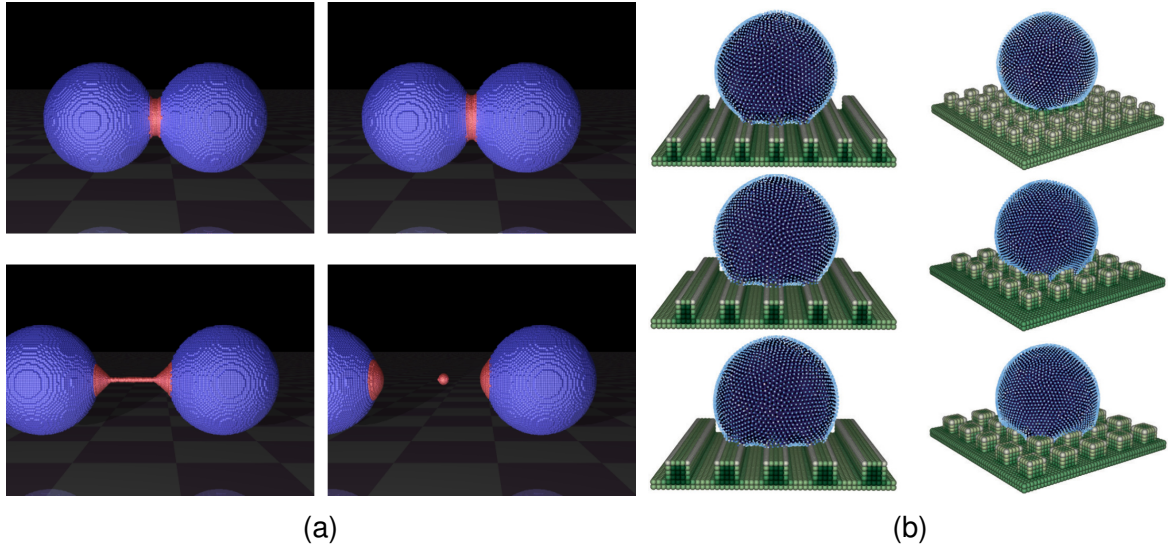


Figure 2: Simulation of capillary phenomena using smoothed particle hydrodynamics (SPH). The image on the right taken from [4] shows the different apparent contact angles observed for different kinds of rectangular gratings on the substrate. Image on the left is result of our simulations showing formation and rupture of liquid bridge between two solid spheres that collide and depart [2].

This work presents several dynamic capillary phenomena where liquid interacts with complex shaped rigid bodies, where the contact angle manifests due to the balance of inter-particle forces between the different phases. In a recent study [4], the motion and pinning of droplets on inclined micrograted surfaces was extensively studied. This study does not involve explicitly imposed contact angles and the desired contact angle is achieved through energy balance at the phase interfaces. Figure 2 shows our SPH simulation of dynamic capillary phenomena and those of [4] for the wetting of micrograted surfaces using SPH.

In addition to the capillary forces, SPH has several other advantages. A single fluid formulation can be achieved where one of the (lighter) phase's dynamics can be neglected and such free surface simulation [8] can be argued to be closer to air-water systems than simulations with low density ratios. An incompressible version of SPH which ensures strict incompressibility [7] yields accurate results comparable with mesh based approaches [26]. Complex shaped boundaries can be easily handled with SPH [14]. Interfacing fluids with different compressibility treatments is successfully demonstrated using SPH [4]. Other physical phenomena involving phase change and heat transfer such as evaporation and condensation can also be simulated using SPH accurately, thanks to the Lagrangian nature of the method [3].

## 2 Preliminary work

For the proposed project we plan to employ an SPH code that has been in continuous development since 2012 [2], by the applicant of this proposal. The applicant is a post

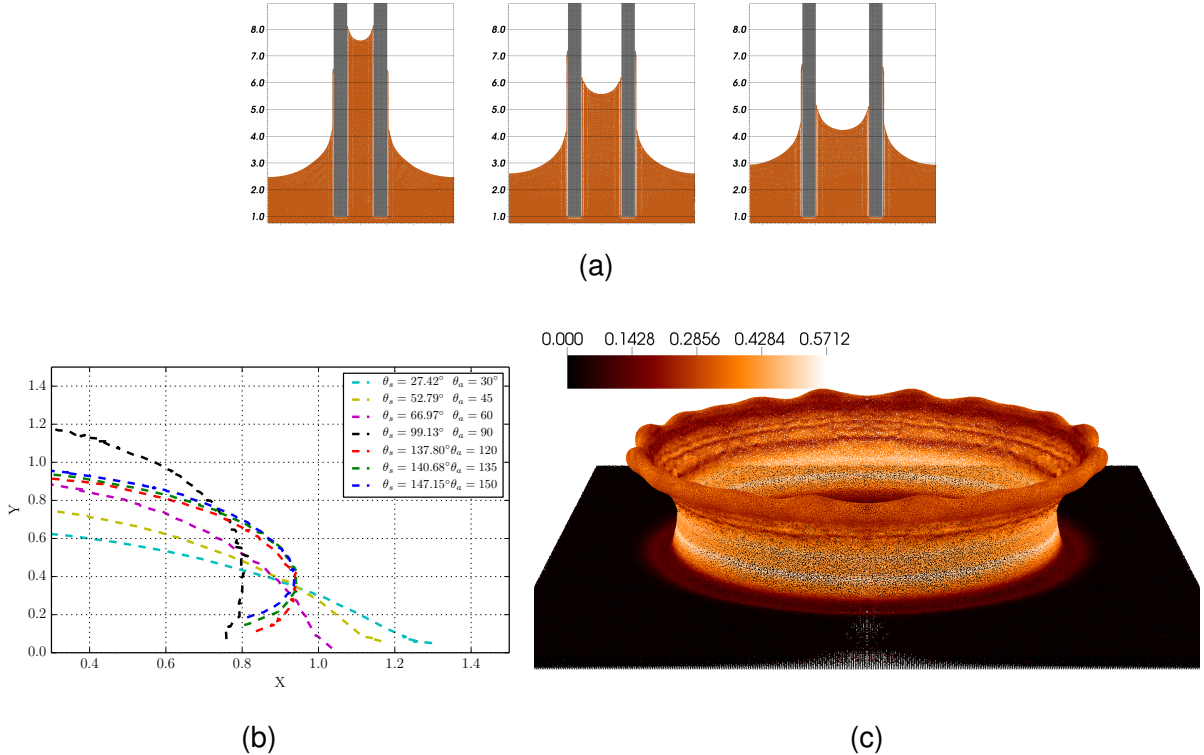


Figure 3: SPH simulations using the pairwise force model for dynamic capillarity: (a) Simulation of 2D capillary rise for different pore diameters (b) Simulated contact interface with different apparent contact angles. (c) 3D simulation of splash crown following impact of drop on a film of liquid, the simulation captures the crown's radial spread accurately and the splash wavelength realistically [2].

doctoral fellow at the Institute for Multiscale Simulation, Friedrich-Alexander University of Erlangen-Nürnberg since 2016. The expertise of the institute in particle based methods and multiscale modelling has been now incorporated into the SPH method [2]. The improved code was successfully applied to a variety of problems, including notoriously difficult systems such as additive manufacturing applications [1].

The SPH program uses a variant of SPH namely incompressible SPH (ISPH) which solves for the condition of isochoricity for incompressibility [7] and can accurately simulate free surface flows [8]. The program has been applied to study fluid-solid interaction problems encountered in water entry of solids of different shapes and density [5] in two and three dimensions. Recently we introduced a dynamic capillary model based on the molecular theory of surface tension to simulate wetting scenarios where capillary, inertial and viscous forces are of comparable time scales [2]. The algorithm was also applied to study liquid bridge formation and rupture [6].

As a preparation for this proposal, we have implemented the following features in this multiphysics SPH program with extensive validation:

- Surface tension using a pairwise force model that recovers the macroscopic surface tension coefficient and contact angle [2].

- Conduction heat transfer across a free surface.
- Phase change using a model that modifies the specific heat near the interface.
- Initial complex geometry input through a triangulated surface geometry file (for example, the STL format).
- High viscosity simulations using an implicit velocity solver, which makes the time step independent of the coefficient of viscosity.
- An improved free surface algorithm that semi-analytically applies Dirichlet boundary conditions at free surfaces and two phase interfaces where only one phase is solved for, enabling the breakup of domain and other interfacial phenomena to be simulated more accurately and robustly [8]. This also allows for pressure gradients tangential to the free surface close to the free surface in contrast to other SPH codes available for academic use.
- Non-uniform interfacial tension by separate Marangoni force model.
- A volume conserving pressure equation is used, which ensures incompressibility is better satisfied, without compromising on efficiency [7, 9].
- The code can also handle rigid and primitively defined bodies [5] with 6 degrees of freedom.
- Species concentration equation and reaction diffusion equation can be added to the set of governing equations without major modifications.

We have performed a number of validation cases to ensure the accuracy of the current code.

Figure 3 shows different simulation results from the implementation of a pairwise force model for surface tension for various interfacial flow phenomena. In Fig. 3a, the capillary rise is validated against theoretical results. The three phase contact angle, which is a macroscopic parameter is recovered with good accuracy from the pair-wise force model (see Fig. 3b). Contact angles are also relevant for the modeling of thin films as the approaching bubbles maintain a certain contact angle depending on the interaction between the air-liquid interfaces. A shared memory parallel simulation of a splash caused by the impact of a droplet on a thin liquid film is shown in Fig. 3c. This recent result shows accurate prediction of the instability that leads to a “crown” formation following the splash. The number of waves on the crown corresponds to experimental observations for the same film Weber number. The use of particle method also enables study of material migration and locally unsteady phenomena.

The liquid phase is modelled here using a one-fluid formulation, neglecting the presence of air and is governed by the incompressible Navier–Stokes equation given by:

$$\frac{d\vec{u}}{dt} = -\frac{1}{\rho}\nabla P + \nabla \cdot \left( \frac{\mu}{\rho}\nabla \vec{u} \right) + \vec{f}^{\text{int}} + \vec{f}^{\text{B}}. \quad (3)$$

Here  $P$  is the pressure,  $\mu$  is the coefficient of viscosity,  $\vec{f}^{\text{int}}$  is the interfacial force acting at the free surface and at the liquid–solid interface and  $\vec{f}^{\text{B}}$  is the body force per unit mass acting on the system. The hydrodynamic pressure is  $P = p + \tilde{p}$ , where  $\tilde{p}$  is a background or ambient constant pressure which does not contribute to the pressure gradient force due to incompressibility of the medium. The pressure  $p$  is not coupled

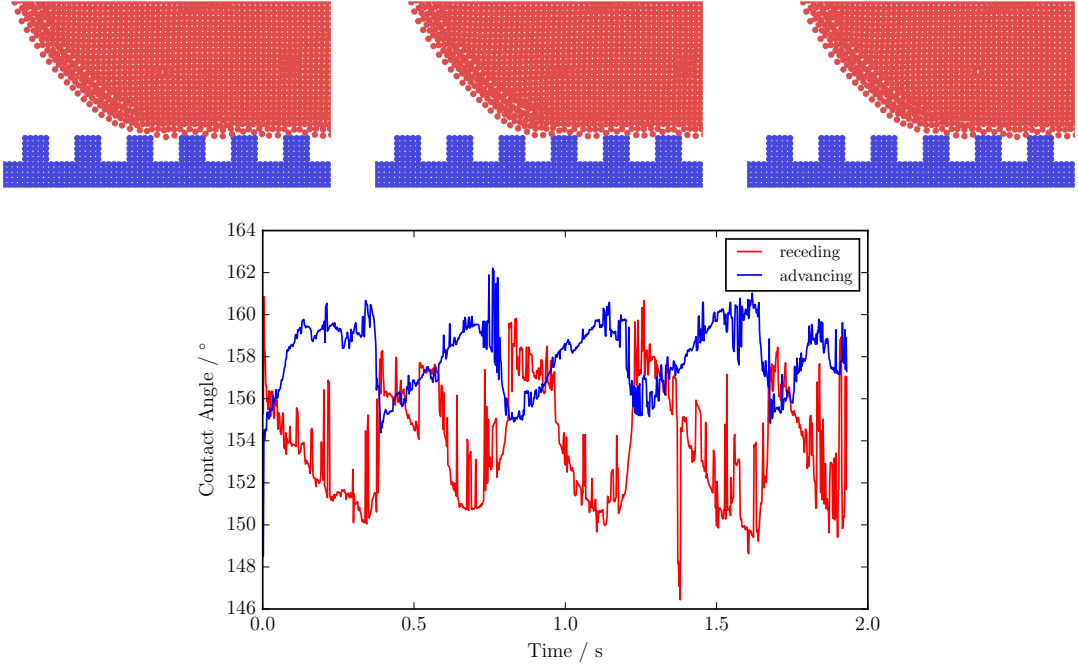


Figure 4: Simulation showing the stick shift behavior of apparent contact angles as a drop moves over a grated surface. The top row shows the instance of receding edge sliding from first to the second image and the jump from one grating to the other in the third image when the receding contact angle undergoes a sharp change. Bottom plot shows the variation of the contact angles over time.

to the density and serves to ensure an incompressibility constraint such as a zero divergence velocity field

$$\nabla \cdot \mathbf{u} = 0, \quad (4)$$

or equivalently, an isochoric deformation given by a unit determinant of deformation gradient tensor  $\vec{F}$  [7]

$$\det(\vec{F}) = 1. \quad (5)$$

The free surface of the fluid and its intersection with a solid surface (called the contact line) are subject to capillary forces modelled as inter-particle forces.

Figure 4 shows the simulation of a 2D drop sliding over a micro grated surface. A bubble of about 1 mm width sliding over microgratings of width 100 micrometers is shown. The microgratings modify the average contact angle measurable using an experimental technique. Whereas the simulation shows the instantaneous configuration of the drop. In Fig. 4, we see that as the drop slides through a flat part of the grating, the apparent contact angle remains the same. However, as the drop moves further, the receding edge jumps from one grating to the other causing an abrupt change in its apparent contact angle. This stick-shift motion is shown in graph at the bottom of this figure. Simulations thus reveal the micromechanics with a greater resolution than experiments. A particle simulation like ours is free from heuristic input parameters and therefore captures the dynamics in way that resembles nature.

## 2.1 List of project-related publications

### 2.1.1 Articles which at the time of proposal submission have been published or officially accepted by publication outlets with scientific quality assurance, listed in standard format; and book publications

- [1] M. Blank, P. Nair, and T. Pöschel. "Capillary viscous flow and melting dynamics: Coupled simulations for additive manufacturing applications". In: *International Journal of Heat and Mass Transfer* (2018), Accepted.
- [2] P. Nair and T. Pöschel. "Dynamic capillary phenomena using Incompressible SPH". In: *Chemical Engineering Science* 176 (2018), pp. 192–204.
- [3] N. Agrawal, P. Nair, T. Pöschel, and S. Roy. "Isotropy of sphere packings in a cylindrical confinement". In: *Chemical Engineering Journal* (2018).
- [4] P. Nair and G. Tomar. "Simulations of gas-liquid compressible-incompressible systems using SPH". In: *Computers & Fluids* 179 (2018), pp. 301–308.
- [5] P. Nair and G. Tomar. "A study of energy transfer during water entry of solids using incompressible SPH simulations". In: *Sādhanā* 42.4 (2017), pp. 517–531.
- [6] P. Nair and T. Pöschel. "Structural changes in wet granular matter due to drainage". In: *EPJ Web of Conferences*. Vol. 140. EDP Sciences. 2017, p. 09005.
- [7] P. Nair and G. Tomar. "Volume conservation issues in incompressible smoothed particle hydrodynamics". In: *J Comp. Phys.* 297 (2015), pp. 689–699.
- [8] P. Nair and G. Tomar. "An improved free surface modeling for incompressible SPH". In: *Comput. & Fluids* 102 (2014), pp. 304–314.

### 2.1.2 Other publications

- [1] M. U. Blank. "Dynamics of melting solids using SPH". Masters thesis. Friedrich-Alexander Universität Erlangen-Nürnberg, 2017.
- [2] P. Nair. "Modeling Free Surface Flows and Fluid Structure Interactions using Smoothed Particle Hydrodynamics". PhD thesis. Bangalore: Department of Mechanical Engineering, Indian Institute of Science, 2015.

### 2.1.3 Patents

- not applicable

### 3 Objectives and deliverables

#### 3.1 Anticipated total duration of the project

- 3 + 3 years. This proposal is for the first phase—3 years.

#### 3.2 Objectives

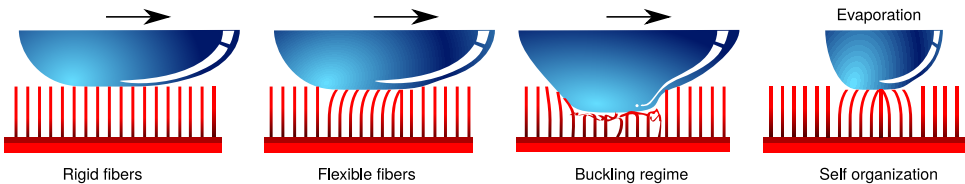


Figure 5: Schematic showing the different flow and fiber deformation regimes considered in this project. The arrow shows the direction of motion of the drop resulting in contact angle hysteresis.

The project aims at optimizing HAR microstructures (also known as micropillar substrates), in terms of pillar density, aspect ratio and bending strength, for increased hydrophobicity and reduced hysteresis, using three dimensional particle based meshless simulations.

Incompressible single component fluid (with a free surface) interacting with deformable, complex shaped solid substrates will be simulated by meshless discretization of the continuum description. The HAR microstructures will be modelled as a chain of particles, similar to the ropes modelled in ship mooring simulations in [8] with bending resistance as a mechanical parameter. The interface forces, both surface tension and wetting, will manifest as a result of inter particle forces between the particles representing the liquid as well as between particles representing the liquid and the solid. The usage of a single line of particles to model HAR would allow us to simulate a large number of pillars in 3D.

The simulations are aimed at providing quantitative relationships between microstructure mechanical properties and the dynamic contact angles. Further, we aim to propose optimal HAR microstructure designs for different wetting regimes. As part of a priority program this project has the advantage of testing and validating the simulations against fabricated experimental surfaces. Also, experimental projects in this direction would help us to reduce the parameter space to investigate.

In Fig. 5 we show the different droplet wetting regimes we expect for different assumed situations. We start with the study of wetting of rigid micropillar arrays, introduce bending of the pillars, consider the cases where the pillars are in a buckled state. Finally we focus on the aggregation and self organization of the pillars due to evaporation or translation of the droplet as is evidenced through experiments in literature. We organize the research plan for the first 3 years into work packages with their respective sets of deliverables.

### 3.3 Work programme including proposed research methods

Our plan for relating micropillar geometry and strength properties to dynamic wetting regimes can be broadly divided into three subsequent work packages and is described below.

#### a) Work package # 1 (WP1)

##### Rigid micropillar array

**Duration:** 0.5 years

Based on the confidence we have from our proof of concept simulations described in Sec. 2 and shown in Fig. 4, we readily propose to simulate motion of droplets of length scale below the capillary length scale given by

$$L_c = \sqrt{\gamma/(\rho g)}, \quad (6)$$

where  $\gamma$ ,  $\rho$  and  $g$  are, respectively, the surface tension coefficient, density of liquid and acceleration due to gravity. For different aspect ratio and consequently different solid area fraction of wetting, we check for the equilibrium contact angle and the apparent advancing and receding contact angles. The drop's Reynolds number will be set to low values. Due to evidence in literature that the receding contact angle has a dependence on inertia in the system [11], we plan to not assume a strict Stoke's regime. Also, we have observed stick-shift motion of the drops with complex detachment and attachment dynamics of the receding contact line. In two dimensions a simulation typically takes one to two days, due to time step restrictions that arise from the capillary time scale, even though the velocity of the drop may be low. In 6 months we plan to complete a parameter study in two dimensions and also perform 3D simulations based on interesting regimes observed in 2D.

#### b) Work package # 2 (WP2)

##### Flexible micropillar array

**Duration:** 1.5 years

During the second work package we plan to extend the understanding we have on the wetting of micropillar arrays when rigid pillars were assumed. The pillars, modelled as a chain of particles which interact with the fluid through potential forces will be given a bending resistance. The chain forming each pillar preserves its length during the deformation. However, its curvature will be computed and resistance to the bending will be assigned according to elastic property of the material simulated.

We plan to replicate micropillars that are practically feasible to prepare. For example, we start with the strength properties of epoxy micropillars as used in [18]. The flexural modulus of epoxy resins is in the range of 10 GPa. We plan to use this value as a reference value and move down to the flexural modulus of hydrogels ( $\approx 100$  kPa) [10]. The use of hydrogels is motivated by the application to tissue engineering. Hydrogels have the advantage of biocompatibility, softness and porous nature [18]. Other materials commonly used for fabricating micropillars are hard polydimethylsiloxane (h-PDMS) (1 MPa) and polypropylene (PP) (150 MPa) [7]. These four materials vis epoxy, PP, h-PDMS and hydrogels, thus span a large range of flexural modulus. Interestingly

it is known that the water holding property of h-PDMS is 20% larger than that of PP, suggesting that softer materials may exhibit greater pinning. However at high aspect ratio both materials displayed higher hydrophobicity. In buckled state, the PP pillars displayed lower hysteresis.

The large range of bending resistance we plan to consider, 100 kPa to 10 GPa, can be possible to simulate due to our simplification of the pillars to a single line of particles, with appropriate flexural modulus. How the time step restriction will affect the feasibility of our simulations needs to be found out. However, we are confident that a large range can be considered representing a variety of materials that are being used for micropillar fabrication today.

At the end of this WP, we plan to deliver the variation of wetting parameters across microstructure topology and material properties. We hope to identify optimal spots in the parameter space in terms of liquid hold up, reversibility and self cleaning properties.

### c) Work package # 3 (WP3)

#### **Effect of drop dynamics on aggregation of micopillars**

**Duration:** 1 years

It is known that flexible micropillars aggregate due to capillary and other electrostatic forces. In this work package we plan to study the effect of drop deformation, either due to its flow dynamics, drop coalescence or due to evaporation of the drop. This is important for reusability of a surface that undergoes wetting. In this work package we plan to model evaporation of drop. SPH being a Lagrangian method makes it easy to model evaporation, as this amounts to losing particles at a desired rate. Marangoni convection may become important in this step. Our code is capable of simulating currents due to temperature gradients and this has been validated against analytical results. An evaporation sessile drop on a micopillar array of flexible pillars will be simulated to observe the feature width of aggregated pillars. Specifically we would like to observe how the droplet splits due to the various instabilities that may be inherent in the system and how each of these sub-droplets contribute to the self organization of the micro pillars.

We also plant to introduce other dynamic scenarios. Two 3D drops will be placed on a micropillar array to check for the underlying aggregation of pillars and how it affects the coalescence and possibility the jumping of these coalesced drops due to hydrophobicity [6].

A self cleaning scenario can be modeled using debris particles that lie between the hairs with a some static charge. The removal of these droplets during the rolling of a droplet can also be studied. Lastly we would like to study the aggregation and self assembly of hairs that are in the trail of a drop moving over the micropillar array. All these simulations will be performed on computers at the Friedrich-Alexander University of Erlangen, where we have simultaneous access to up to 500 compute nodes at a time.

#### **Possible plan for extension to second phase**

If granted, and provided the first phase of the project goes according to plan, the second phase of the project will focus on the effect of switching and tuning of the microstructure to control motion of droplets .

Year	1				2				3			
Quarter	1	2	3	4	1	2	3	4	1	2	3	4
WP1: Rigid pillars												
WP2: Flexible pillars												
WP3: Drop dynamics and pillar aggregation												

Table 0.1: The timeline planned for different work packages in the project

### 3.4 Data handling

The primary way to disseminate the results of our research will be through scientific publications in refereed journals. The computer code(s) we use for the simulations are currently version controlled through the version control software, GIT. This makes it easy for publishing the code as an open source project through websites such as github or bitbucket.

### 3.5 Other information

- not applicable

### 3.6 Explanations on the proposed investigations

#### 3.6.1 Experiments involving humans or human materials

- not applicable

#### 3.6.2 Animal experiments

- not applicable

### 3.7 Involvement of international cooperation partners

- not applicable

## 4 Bibliography

- [1] M. U. Blank. “Dynamics of melting solids using SPH”. Masters thesis. Friedrich-Alexander Universität Erlangen-Nürnberg, 2017.
- [3] A. Farrokhpourah, M. Bussmann, and J. Mostaghimi. “New smoothed particle hydrodynamics (SPH) formulation for modeling heat conduction with solidification and melting”. In: *Numerical Heat Transfer, Part B: Fundamentals* 71.4 (2017), pp. 299–312.

- [4] E. Shigorina, J. Kordilla, and A. M. Tartakovsky. "Smoothed particle hydrodynamics study of the roughness effect on contact angle and droplet flow". In: *Physical Review E* 96.3 (2017), p. 033115.
- [5] F. O. Alpak, B. Riviere, and F. Frank. "A phase-field method for the direct simulation of two-phase flows in pore-scale media using a non-equilibrium wetting boundary condition". In: *Computational Geosciences* 20.5 (2016), pp. 881–908.
- [6] X. Chen, R. S. Patel, J. A. Weibel, and S. V. Garimella. "Coalescence-induced jumping of multiple condensate droplets on hierarchical superhydrophobic surfaces". In: *Scientific Reports* 6 (2016), p. 18649.
- [7] S. Varagnolo, N. Basu, D. Ferraro, T. Toth, M. Pierno, G. Mistura, G. Fois, B. Tripathi, O. Brazil, and G. Cross. "Effect of hair morphology and elastic stiffness on the wetting properties of hairy surfaces". In: *Microelectronic Engineering* 161 (2016), pp. 74–81.
- [8] S. Lind, P. Stansby, and B. Rogers. "Fixed and moored bodies in steep and breaking waves using SPH with the Froude–Krylov approximation". In: *Journal of Ocean Engineering and Marine Energy* 2.3 (2016), pp. 331–354.
- [9] T. L. Liu, Z. Chen, and C.-J. Kim. "A dynamic Cassie–Baxter model". In: *Soft Matter* 11.8 (2015), pp. 1589–1596.
- [10] M. Czerner, L. S. Fellay, M. P. Suárez, P. M. Frontini, and L. A. Fasce. "Determination of elastic modulus of gelatin gels by indentation experiments". In: *Procedia Materials Science* 8 (2015), pp. 287–296.
- [2] P. Nair. "Modeling Free Surface Flows and Fluid Structure Interactions using Smoothed Particle Hydrodynamics". PhD thesis. Bangalore: Department of Mechanical Engineering, Indian Institute of Science, 2015.
- [11] J. Wang, M. Do-Quang, J. J. Cannon, F. Yue, Y. Suzuki, G. Amberg, and J. Shiomi. "Surface structure determines dynamic wetting". In: *Scientific Reports* 5 (2015), p. 8474.
- [9] P. Nair, A. Vijayakumar, and G. Tomar. "A Deformation Gradient based formulation for Incompressible Smoothed Particle Hydrodynamics". In: *Proc. 14th Asian Congress of Fluid Mechanics, Hanoi, Vietnam*. Oct. 2013.
- [12] J. S. Rowlinson and B. Widom. *Molecular theory of capillarity*. Courier Corporation, 2013.
- [13] P. M. Kulkarni, C.-C. Fu, M. S. Shell, and L. Gary Leal. "Multiscale modeling with smoothed dissipative particle dynamics". In: *Journal of Chemical Physics* 138.23 (2013), p. 234105.
- [14] M. Ferrand, D. Laurence, B. D. Rogers, D. Violeau, and C. Kassiotis. "Unified semi-analytical wall boundary conditions for inviscid, laminar or turbulent flows in the meshless SPH method". In: *International Journal for Numerical Methods in Fluids* 71.4 (2013), pp. 446–472.
- [15] C. Duprat, S. Protiere, A. Beebe, and H. Stone. "Wetting of flexible fibre arrays". In: *Nature* 482.7386 (2012), p. 510.
- [16] X.-F. Wu, A. Bedarkar, and K. A. Vaynberg. "Droplets wetting on filament rails: Surface energy and morphology transition". In: *Journal of Colloid and Interface Science* 341.2 (2010), pp. 326–332.

- [17] O. Desjardins and V. Moureau. "Methods for multiphase flows with high density ratio". In: *Center for Turbulent Research, Summer Programm* 2010 (2010), pp. 313–322.
- [18] D. Chandra and S. Yang. "Stability of high-aspect-ratio micropillar arrays against adhesive and capillary forces". In: *Accounts of Chemical Research* 43.8 (2010), pp. 1080–1091.
- [19] A. Bedarkar, X.-F. Wu, and A. Vaynberg. "Wetting of liquid droplets on two parallel filaments". In: *Applied Surface Science* 256.23 (2010), pp. 7260–7264.
- [20] S. T. Larsen and R. Taboryski. "A Cassie-like law using triple phase boundary line fractions for faceted droplets on chemically heterogeneous surfaces". In: *Langmuir* 25.3 (2009), pp. 1282–1284.
- [21] M. Reyssat and D. Quéré. "Contact angle hysteresis generated by strong dilute defects". In: *Journal of Physical Chemistry B* 113.12 (2009), pp. 3906–3909.
- [22] A. A. Saha and S. K. Mitra. "Effect of dynamic contact angle in a volume of fluid (VOF) model for a microfluidic capillary flow". In: *Journal of Colloid and Interface Science* 339.2 (2009), pp. 461–480.
- [23] R. Chen, M.-C. Lu, V. Srinivasan, Z. Wang, H. H. Cho, and A. Majumdar. "Nanowires for enhanced boiling heat transfer". In: *Nano letters* 9.2 (2009), pp. 548–553.
- [24] C. Dorrer and J. Rühe. "Some thoughts on superhydrophobic wetting". In: *Soft Matter* 5.1 (2009), pp. 51–61.
- [25] M. T. Northen, C. Greiner, E. Arzt, and K. L. Turner. "A Gecko-inspired reversible adhesive". In: *Advanced Materials* 20.20 (2008), pp. 3905–3909.
- [26] E.-S. Lee, C. Moulinec, R. Xu, D. Violeau, D. Laurence, and P. Stansby. "Comparisons of weakly compressible and truly incompressible algorithms for the SPH mesh free particle method". In: *Journal of Computational Physics* 227.18 (2008), pp. 8417–8436.
- [27] C. Dorrer and J. Rühe. "Drops on microstructured surfaces coated with hydrophilic polymers: Wenzel's model and beyond". In: *Langmuir* 24.5 (2008), pp. 1959–1964.
- [28] H.-M. Kwon, H.-Y. Kim, J. Puëll, and L. Mahadevan. "Equilibrium of an elastically confined liquid drop". In: *Journal of applied physics* 103.9 (2008), p. 093519.
- [29] H. Ding and P. D. Spelt. "Wetting condition in diffuse interface simulations of contact line motion". In: *Physical Review E* 75.4 (2007), p. 046708.
- [30] X.-M. Li, D. Reinhoudt, and M. Crego-Calama. "What do we need for a superhydrophobic surface? A review on the recent progress in the preparation of superhydrophobic surfaces". In: *Chemical Society Reviews* 36.8 (2007), pp. 1350–1368.
- [31] J. J. Monaghan. "Smoothed particle hydrodynamics". In: *Reports on Progress Physics* 68.8 (2005), p. 1703.
- [32] T. N. Krupenkin, J. A. Taylor, T. M. Schneider, and S. Yang. "From rolling ball to complete wetting: the dynamic tuning of liquids on nanostructured surfaces". In: *Langmuir* 20.10 (2004), pp. 3824–3827.

- [33] N. Kaji, Y. Tezuka, Y. Takamura, M. Ueda, T. Nishimoto, H. Nakanishi, Y. Horiike, and Y. Baba. "Separation of long DNA molecules by quartz nanopillar chips under a direct current electric field". In: *Analytical Chemistry* 76.1 (2004), pp. 15–22.
- [34] D. Gueyffier, J. Li, A. Nadim, R. Scardovelli, and S. Zaleski. "Volume-of-fluid interface tracking with smoothed surface stress methods for three-dimensional flows". In: *Journal of Computational Physics* 152.2 (1999), pp. 423–456.
- [35] W. Barthlott and C. Neinhuis. "Purity of the sacred lotus, or escape from contamination in biological surfaces". In: *Planta* 202.1 (1997), pp. 1–8.
- [36] J. Joanny and P.-G. De Gennes. "A model for contact angle hysteresis". In: *Journal of Chemical Physics* 81.1 (1984), pp. 552–562.
- [37] H. Princen. "Capillary phenomena in assemblies of parallel cylinders: II. Capillary rise in systems with more than two cylinders". In: *Journal of Colloid and Interface Science* 30.3 (1969), pp. 359–371.
- [38] A. Cassie and S. Baxter. "Wettability of porous surfaces". In: *Transactions of the Faraday Society* 40 (1944), pp. 546–551.

## 5 Requested modules/funds

### 5.1 Basic Module

#### 5.1.1 Funding for staff

With this proposal, the applicant requests funding for his own position (Temporary Position for Principal Investigator). Given on his experiences in the field of research obtained during his PhD research at the Indian Institute of Science in Bangalore and during his postdoctoral studies at the Institute for Multiscale Simulation at the University Erlangen-Nuremberg, the applicant is well prepared for performing the proposed research project.

The postdoctoral researcher, shall be supported by a student helper (WiHi with bachelor degree). The student helper will support the researcher with performing routine simulations, analyze the simulation results and care for Data Handling (see. 2.4).

Therefore, we request the following funding for staff:

#### Temporary Position for Principal Investigator

- Dr. Prapanch Nair (TV-L E13 Stufe 2 bis E14 Stufe 1), 100%
- duration: 36 months
- requested funds:  $36 \text{ months} \times 5\,825 \text{ €} (\text{per month}) = 209\,700 \text{ €}$

#### 5.1.1.1 Student helper (WiHi)

- N.N. 80 hours/month : €2262.5 per month)

- duration: 36 months
- requested funds:  $36 \text{ months} \times €2262.5 \text{ (per month)} = €81450$

**Total requested funding for staff: €291150**

### 5.1.2 Direct project costs

#### 5.1.2.1 Equipment up to €10,000, software and consumables

1. data storage (hard discs), 1 000 € p.a.	3 000€
--	--------

Total	3 000€
-------	--------

#### 5.1.2.2 Travel Expenses

1. 2 conferences overseas, each one 1200 € transport, 4600€ 500 € hotel, 600 € conference fee
2. 2 conferences in Germany and Europe, each one 2000€ 700 € transport and hotel, 300 € conference fee

Total	6600€
-------	-------

#### 5.1.2.3 Visiting Researchers

- not applicable

#### 5.1.2.4 Expenses for Laboratory Animals

- not applicable

#### 5.1.2.5 Other costs

- not applicable

#### 5.1.2.6 Project-related publication expenses

- 750€ p.a. = 2250€ for 3 years

#### 5.1.2.7 Instrumentation

- not applicable

**Total requested funding for direct project costs: €12,350**

## **6 Project requirement**

### **6.1 Employment status information**

The applicant, Dr. Prapanch Nair, is currently employed as a postdoctoral fellow at the Institute for Multiscale Simulation at the Friedrich Alexander Universit"at Erlangen-Nuremberg, Department for Biological and Chemical Engineering (CBI). The current contract ends October 31, 2019.

### **6.2 First time proposal data**

- not applicable

### **6.3 Composition of the project group**

The proposed research will be performed at the Institute for Multiscale Simulation. With the following colleagues from this institute exist collaborations or concrete plans for collaboration in relation with the current proposal:

- Prof. Dr. T. Pöschel (head of the institute)
- Prof. Dr. M. Engel (particle simulation)
- Dr. P. Müller - permanent staff member (particle-fluid coupling)
- Dr. Daniel Nasato - DFG-SFB-funded (DEM simulation)
- Dr. Christopher Robert Windows-Yule - non-permanent staff member (Statistical mechanics of particle systems)
- Dr. Mubashir Hussain - non-permanent staff member (particle based fluid simulations)
- Dipl.-Ing. Sebastian Mühlbauer - DFG-funded (chemical reaction kinetics)

### **6.4 Cooperation with other researchers**

#### **6.4.1 Researcher with existing cooperation agreement for the present project**

For the priority programme SPP 2171, we plan to collaborate with other projects in the program that fall under the following categories:

- Experimental research focused on measurement of contact angles on substrates made of soft/elastic material microstructure.
- Experimental research focused on dynamic measurement of receding contact angles, as we intend to simulate and measure the same.
- Simulations that model drop motion at the macro scale which could couple our micro scale findings for larger simulations.

- Experimental research that characterizes substrate topology.

Apart from the researchers from the Institute for Multiscale Simulations and other groups participating in SPP 2171, there is ongoing collaboration with

- Prof. Dr. J. Harting, FAU Erlangen, Institute for Complex Fluids and Interfaces
- Prof. Dr. U. Rüde, FAU Erlangen, Institute for Computer Science

#### **6.4.2 Researcher with whom collaboration was done in the past three years (only fields related to the current research project)**

Prof. N. Brilliantov (Univ. Leicester); Prof. A. Formella (Univ. Vigo); Prof. J. Harting (Univ. Erlangen); Prof. J. Gallas (Univ. Joao Pessoa); Dr. P. Nair (Univ. Erlangen); Prof. S. Roy (IIT Delhi, India); Prof. G. Tomar (IISc Bangalore, India).

### **6.5 Scientific equipment**

The Institute for Multiscale Simulation has a medium size Linux cluster with about 800 cores which can be used for simulations. Larger simulations shall be performed at the computer center of the university (RRZE-Regionales Rechenzentrum Nürnberg) where the institute has a contingent of computer time.

### **6.6 Project-relevant cooperation in commercial enterprises**

- not applicable

### **6.7 Project-relevant participation in commercial enterprises**

- not applicable

## **7 Additional information**

- No funding request for this project has been previously submitted to any third party. In case such a request is submitted, the German Research Foundation will be immediately informed.
- The DFG Liaison Officer has been informed of this application



# PRAPANCH NAIR

## PERSONAL INFORMATION

DOB	06 October, 1985
nationality	Indian
address	Nürnberg Str. 83, 91052 Erlangen, Germany
email	<a href="mailto:prapanch.nair@fau.de">prapanch.nair@fau.de</a>
phone	(M) +49 15223231459 · (H) +49 15259336409

## RESEARCH EXPERIENCE

*Feb'16–till date* Post Doctoral Fellow

*Institute for  
Multiscale  
Simulation,  
Friedrich-  
Alexander  
Universität  
Erlangen-  
Nürnberg*

- *Multiphysics in additive manufacturing*  
Development of multiphysics meshless solver for coupled laser radiation, heat transfer, fluid flow and phase change problems, based on smoothed particle hydrodynamics (sph).
- *Coordinator, ugc-daad project: deep conversion in packed bed reactors*  
Investigation of effect of catalyst pellets packing on the performance of trickle-bed reactors. The study applies various numerical techniques: ballistic deposition of particles, sph and fvm, and experimental methods: resin filling and x-ray tomography of packings.
- *Micromechanics of unsaturated wet granular media*  
Development of interface models in mesh free methods; applying them to solve dynamics of wet unsaturated media.
- *Wetting phenomena*  
Development of novel wetting models in meshfree methods; applying them to solve interaction of liquids with surfaces of different wetting properties.
- *HPC development*  
Performance improvements of snusph—in-house isph code—for accessing the computing power of heterogenous clusters. Focus on SIMD (vectorization) aware code and libraries.

*Jul'15-Jan'16* Research Associate

*Indian Institute of  
Science, Bangalore*

*Dept. of Mechanical Engineering*  
Developed a FVM solver for two phase flows for application to multiscale problems

*Aug'10-Jul'15* Ph.D.

*Indian Institute of  
Science, Bangalore*

GPA: 6.3/8.0 · *Dept. of Mechanical Engineering*  
Developed SNUSPH: An Incompressible Smoothed Particle Hydrodynamics (ISPH) Code with free surface modeling, multiphase, rigid body interactions, elastic membrane interactions and surface tension. Implementation of version control and OpenMP parallelization of SNUSPH. Applied the code for solving problems in water-entry of rigid bodies, fluid structure interaction and multiphase flows involving compressible and incompressible phases.

Introduced an accurate and efficient free surface model for ISPH method. Improved a surface tension model based on Moving Least Squares algorithm to reconstruct interfaces and further extended to model elastic membranes. Identified a volume conservation issue that particle methods suffer from, and introduced an improved pressure model.

*Feb–April '10* Scientist-C

*Indian Space  
Research  
Organization*

Developed a Earth coordinate transform tool to switch between various coordinate systems used in space mechanics.

*Mar'09–Feb'10* Scientist/Engineer

RWDI India Pvt.  
Ltd.

Used OpenFOAM to study natural convection in micro-climates. Studied wind loads on chimneys and buildings. Proposed wind-dower design modifications based on CFD studies. Developed snow flake transport model in OpenFOAM.

Anna University,  
Tamilnadu, India.

2003–2007              Bachelor of Engg., Aeronautical Engineering  
Score 83%   · Park College of Engg. & Technology  
Proposed an artificial entropy correction for FVM solutions of hyperbolic Partial Differential Equations for the final year project.

#### JOURNAL PUBLICATIONS

Michael BLANK, Prapanch NAIR, Thorsten PÖSCHEL, "Capillary viscous flow and melting dynamics: Coupled simulations for additive manufacturing applications," *International Journal of Heat and Mass Transfer*, 2018. (*Accepted, in print*).

Prapanch NAIR, Gaurav TOMAR, "Simulations of gas-liquid compressible-incompressible systems using SPH," *Computers & Fluids*, 2018.

Nikhil Agrawal, Prapanch Nair, Thorsten Pöschel, Shantanu Roy, "Isotropy of sphere packings in a cylindrical confinement," *Chemical Engineering Journal*, 2018.

Prapanch NAIR, Thorsten PÖSCHEL, "Dynamic Capillary phenomena using ISPH," *Chemical Engineering Science* 176 (2018) 192–204

Prapanch NAIR, Gaurav TOMAR, "A study of energy transfer during water entry of solids using incompressible SPH simulations, *Sdhan* 42.4 (2017) 517531.

Prapanch NAIR, Gaurav TOMAR, "Volume Conservation issues in Incompressible Smoothed Particle Hydrodynamics (ISPH)," *Journal of Computational Physics* 297 (2015) 689 – 699.

Prapanch NAIR, Gaurav TOMAR, "An improved free surface modeling for incompressible SPH," *Computers and Fluids* 102 (2014) 304 – 314.

#### CONFERENCE PRESENTATIONS AND PROCEEDINGS

Powders & Grains

July, 2017   · Montpellier, France.  
Structural changes in wet granular matter due to drainage  
Authors: Prapanch NAIR, Thorsten PÖSCHEL

12th International SPHERIC workshop

June, 2017   · Ourense, Spain.  
Rounding of a melting particle  
Authors: Prapanch NAIR, Michael BLANK, Thorsten PÖSCHEL

42nd National Conference on Fluid Mechanics and Fluid Power

December 2015   · NITK Suratkal, India.  
A study of water entry of rigid bodies using Incompressible Smoothed Particle Hydrodynamics  
Authors: Prapanch NAIR, Gaurav TOMAR

14th Asian Congress of Fluid Mechanics

October 2013   · Hanoi, Vietnam  
A Deformation Gradient based formulation for Incompressible Smoothed Particle Hydrodynamics  
Authors: Prapanch NAIR, Adithya VIJAYAKUMAR, Gaurav TOMAR

5th National Conference on Wind Engineering

November 2009   · Surat, India  
Application of CFD in Stack Interference  
Authors: Prapanch NAIR, Suresh KUMAR, Jon GALSWORTHY

#### MENTORING

Students

2018   · PhD Student  
Instabilities in melt pool due to laser heating of metals and polymers  
2018   · Two masters students working on packings of complex shaped particles in chemical reactors

2017 · Master's Theses  
 Heat transfer and phase change in additive manufacturing applications  
 2017 · Exchange student (Master's)  
 Characterizing packing of reactor beds—experiments and computations

*Lecturing*                    2017 · IIT Delhi  
 Four day introductory lecture on meshless methods  
 2013,14 · Coimbatore, India  
 Crash course for GATE entrance exam candidates

#### COMPUTATIONAL SKILLS

<i>Languages</i>	C++	Advanced C	Python	Fortran
<i>Software/Libraries</i>	Linux	OpenMP	GERRIS	GIT
	MPI	Torque-PBS	OpenFOAM	SLURM
	VTK	CUDA	OpenCL	PovRAY
	Json	xml	vtk	Matplotlib
	Doxxygen	html/css	gdb	valgrind

#### BELLS & WHISTLES

<i>Positions held</i>	2013 – Elected Sec. Academic Affairs, Students' Council, Indian Institute of Science
	2012 – Communications committee member, Students' Council
	2012 – Convener, Fine Arts Club, Indian Institute of Science
<i>Languages</i>	ENGLISH · HINDI · MALAYALAM · TAMIL
<i>Presentation skills</i>	LAT <sub>E</sub> X · SVG · HTML/CSS · Gimp · Poster/infographic designs
<i>Interests</i>	Pencil sketching · Running · Reading · Typography

#### REFERENCES

<i>FAU, Erlangen.</i>	Prof. Dr. Thorsten Pöschel · Institute for Multiscale Simulation +49 (0)9131 8520867 · <a href="mailto:thorsten.poeschel@fau.de">thorsten.poeschel@fau.de</a>
<i>Fraunhofer Institute (IVI), Dresden.</i>	Dr. Severin Strobl +49 351 4640 818 · <a href="mailto:severin.strobl@ivi.fraunhofer.de">severin.strobl@ivi.fraunhofer.de</a>
<i>Indian Institute of Science, Bangalore.</i>	Dr. Gaurav Tomar · Department of Mechanical Engineering +91 9538240256 · <a href="mailto:gtom@mecheng.iisc.ernet.in">gtom@mecheng.iisc.ernet.in</a>
<i>RWDI India Pvt. Ltd., Trivandrum.</i>	Dr. Suresh Kumar · Director, RWDI India +91 9895976686 · <a href="mailto:suresh@rwdi.com">suresh@rwdi.com</a>

## Arbeitgebererklärung

Der Arbeitgeber Institute for Multiscale Simulation, Friedrich-Alexander-University Erlangen-Nuremberg (Name des Arbeitgebers)

stellt Herrn/Frau Dr. Prapanch Nair

im Falle der Bewilligung seines/ihres Antrags auf die Eigene Stelle durch die Deutsche Forschungsgemeinschaft (DFG) befristet für die Dauer seiner/ihrer Förderung mit der Eigenen Stelle als wissenschaftliche/n Mitarbeiter/in ein. Sie stellt ihm/ihr für diesen Zeitraum die notwendige Grundausstattung (z.B. Laborräume, Büroräume etc.) zur Verfügung. Es gelten die an der Einrichtung einschlägigen Tarifvorschriften mit der Maßgabe, dass

a) sich die Arbeitspflicht von Herrn/Frau Dr. Prapanch Nair

auf sein/ihr von der DFG gefördertes Forschungsvorhaben (Thema)

Optimization of micropillar carpets for reversible wetting using meshless simulations

und damit unmittelbar zusammenhängende wissenschaftliche Dienstleistungen beschränkt und

b) der Arbeitgeber nicht durch dienstliche Anordnungen Einfluss auf die selbständige Bearbeitung des genannten Forschungsvorhabens nimmt.

Die/Der Unterzeichnende bestätigt, dass die für die Unterzeichnung notwendige Befugnis vorliegt und alle notwendigen internen Abstimmungen erfolgt sind.

Erlangen, 15.10.2018

Ort, Datum



Unterschrift und Stempel

Lehrstuhl für  
Multiscale Simulation  
Universität Erlangen-Nürnberg  
Prof. Dr. Thorsten Pöschel  
Nägelsbachstr. 49 b  
D-91052 Erlangen

Prof. Dr. Thorsten Pöschel, Director, chair holder

Name und Funktion der/des Unterzeichnenden

# Capillary viscous flow and melting dynamics: Coupled simulations for additive manufacturing applications

Michael Blank<sup>a</sup>, Prapanch Nair<sup>a,\*</sup>, Thorsten Pöschel<sup>a</sup>,

<sup>a</sup> Institute for Multiscale Simulation, Friedrich-Alexander Universität Erlangen-Nürnberg, Erlangen.

---

## Abstract

The rate of melting of a solid and the rate of deformation of the resulting melt due to capillary forces are comparable in additive manufacturing applications. This dynamic structural change of a melting solid is extremely challenging to study experimentally. Using meshless numerical simulations we show the influence of the flow of the melt on the heat transfer and resulting phase change.

We introduce an accurate and robust Incompressible Smoothed Particle Hydrodynamics (ISPH) method to simulate melting of solids and the ensuing fluid-solid interaction. We present validations for the heat transfer across the free surface and the melting interface evolution, separately. We then present two applications for this coupled multiphysics simulation method—the study of rounding of an arbitrarily shaped particle during melting and the non-linear structural evolution of three spheres undergoing agglomeration. In both the studies we use realistic transport and thermal properties for the materials so as to demonstrate readiness of the method for solving engineering problems in additive manufacturing.

*Key words:* Additive manufacturing, Incompressible Smoothed Particle Hydrodynamics, phase change, latent heat, melting dynamics

---

## 1. Introduction

The evolution of topology in melting system, such as encountered in additive manufacturing applications, is often studied by decoupling the time scales of the flow of the melt and the phase change. Either static material properties are assumed, approximating the solids as highly viscous fluids [15] or assuming no flow following melting [32]. As the scope of additive manufacturing widens, there is an increasing need to resolve the tight coupling between flow of the melt and the phase change in order to achieve expected strength of the material. For serious engineering applications, uniformity in density and strength of the manufactured parts demand a micro mechanical understanding of the structural evolution during successive melting and solidification the material undergoes several times. Experimental studies at such spatial and temporal resolutions may be expensive [10], not to mention the high temperature conditions in which measurements need to be made. Traditional mesh based numerical approaches based on the Eulerian description (such as the Finite Volume Method)

---

\*Principal corresponding author

Email addresses: prapanch.nair@fau.de (Prapanch Nair)

require special interface advection schemes (such as the Volume of Fluid method [12]) for fluid–fluid interfaces and Immersed Boundary [20] methods for evolving fluid–solid interface. These methods are challenged by large density ratios and the need for explicit conservation of mass, respectively. Mesh based methods based on the Lagrangian description (such as the Finite Element Method), on the other hand, are challenged by large deformations that require complex mesh treatments during the course of the simulation [2]. This is inherently due to the need to maintain the neighbor connectivity information between the computational nodes. In either case, generation of an efficient mesh requires considerable time and skill, especially in case of problems with evolving geometries. Meshless methods hold several advantages for such multi-physics applications.

Smoothed Particle Hydrodynamics (SPH) is a meshfree updated-Lagrangian method which was introduced by Gingold and Monaghan [9] and Lucy [17] for treating astrophysical phenomena and gas dynamics. Since the method is free from the need for the mesh connectivity information, many problems with complex interfaces and discontinuities in the domain are effectively solved by the method, making it a practical tool for multiphysics problems. For example, Monaghan presented an impressive SPH simulation of a methane gas bubble toppling a trawler to explain the sinking of ships in Witches Hole in the North sea [18]. This multiphysics simulation coupled two phase flow with free surface to an interacting rigid body. Heat transfer [22], phase change [8], and capillary flows [23] are solved separately using the method and are being continuously applied to a wide variety of engineering problems.

To successfully couple heat transfer, phase change and capillary flows in the context of additive manufacturing applications, each of these modules need to be improved and validated for appropriate boundary conditions (BC). Heat transfer is solved in SPH using the passive scalar approach for temperature [22]. The definition of accurate second order derivatives with discontinuous transport coefficients makes it applicable to realistic problems. Heat transfer from an ambient constant (or time varying) temperature needs to be implemented as a Dirichlet BC for temperature. A thin layer of SPH particles may be used for such BCs, but this would deteriorate the order of accuracy of the method itself. Hence, for problems involving continuous deformation, we present a free surface Dirichlet BC that is quite similar to the free surface Dirichlet BC for pressure in an earlier work [24].

Heat transfer—through conduction and convection due to capillary flow—effects phase change based on the latent heat capacity of the material. Phase change in a static domain has been solved using SPH [8] using a temperature as a passive scalar undergoing diffusion. Enthalpy based formulations have also been used for solving heat transfer in SPH [8] as an alternative approach. However, this involves computations of higher order derivatives than the temperature based approach. Using the free surface Dirichlet BC for temperature, the temperature based heat transfer model is used here to drive the phase change. A suitable capillary force model at the free surface is necessary to drive the flow and thereby cause convective transport of temperature. Capillary forces can be implemented in SPH using either continuum surface force (CSF) based models [1], geometric reconstruction of the interfaces [38] or using pairwise forces [34, 23]. Continuum models were developed for two fluid interfaces, and require special treatment for single fluid formulations with free surfaces [7]. The geometric models require robust, often expensive, reconstruction of interfaces from discrete particles for stable behaviour. For free surfaces we find the pairwise force model to be more amenable, since free surface and wetting phenomena are readily captured using this

approach. Recently, the pairwise force model was applied to dynamic capillary phenomena [23] in the Incompressible SPH (ISPH) method to show how additional damping may result from superimposing molecular length scales on a continuum model, and a restriction on the minimum smoothing resolution that is necessary to avoid this artificial damping. Different dynamic capillary flows involving free surfaces were demonstrated in this work. Other suitable capillary models may also be implemented in this context.

Multiphysics approaches for such tightly coupled phase change problems have also been solved using mesh based methods such as the finite volume method [11] and the finite element method [30, 5, 28]. In [11], the volume of fluid (VoF) method was used to characterize free surfaces of the flow resulting from a laser beam melting (LBM) process. In [28] a selective electron beam melting process, taking into account thermomechanical coupling and high temperature gradients in multiple time and length scales using a continuum assumption for the bed of particles, was considered. However, to our knowledge a melting model that takes into account the fluid-solid interaction with all degrees of freedom of the solids has not been attempted using mesh based methods in the context of additive manufacturing applications. Hence, we find that meshless methods such as SPH, where fluid solid interactions are easier to model owing to inherent mass conservation across the interface, could be a valuable addition. We have limited the scope of the current work to conduction and convection heat transfer (due to the melt flow) and assume negligible thermal gradients and therefore a constant surface tension coefficient. We systematically introduce and validate heat transfer and phase change to the flow solver to eventually solve fully coupled problems within this scope.

This paper is organized as follows. In Sec. 2, we present the heat transfer, phase change and capillary flow models with the respective governing equations. In Sec. 3 we present numerical implementation of these models to the ISPH method. Here we introduce our BC for heat transfer across the free surface. We also separately validate the heat transfer across free surface and the melting of a solid for different latent heat values in 2D and 3D. In Sec. 4 we present applications of this method to representative problems in additive manufacturing. We compare the melting rate of a complex shaped solid particle with theoretical results for the melting of a spherical solid to appreciate the influence of shape on the capillary viscous flow on the heat transfer in the melting particle. Finally, we simulate the agglomeration of a chain of three solid spheres undergoing melting with two different sets of material properties to show the shape evolution is a result of instabilities relating to the solid–liquid interaction during the melting process.

## 2. Governing Equations

We assume the fluid (melt) and the solid to be incompressible, with negligible density variation during the phase change. The transient heat transfer in the system is governed by the enthalpy equation,

$$\frac{\partial H}{\partial t} = \nabla \cdot (k \nabla T), \quad (1)$$

where  $H$  is the enthalpy,  $k$  is the thermal conductivity of the material and  $T$  is the temperature. For an incompressible medium, the enthalpy  $H$  can be written as a function of

temperature. Therefore,

$$\frac{dH}{dT} \frac{\partial T}{\partial t} = \nabla \cdot (k \nabla T). \quad (2)$$

Here  $dH/dT$  is the specific heat capacity at constant pressure,  $C$ .

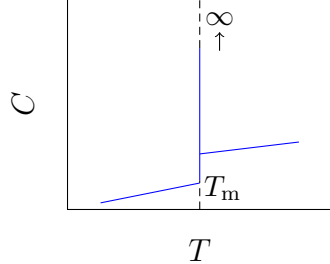


Figure 1: Sketch of the specific heat to temperature dependence during a melting process.

Phase change (melting and solidification) can be modelled using Eq. 2 by defining an effective heat capacity [8] which increases (or decreases) by the latent heat of melting (or solidification),  $L$ , of the material at a melting (or solidifying) interface. This effective heat capacity can be defined as

$$C_{\text{eff}} = \begin{cases} C_s & T < T_m \\ C_m + L\delta(T - T_m) & T = T_m \\ C_l & T > T_m \end{cases} \quad (3)$$

where  $\delta(T - T_m)$  is the Dirac delta function,  $C_s$  and  $C_l$  are the specific heat capacities of the material in the solid and liquid phases, respectively, and  $C_m$  is the specific heat capacity of the material at the melting temperature. This model relating the heat capacity to the temperature and the latent heat is schematically shown in Fig. 1.

The liquid domain formed from the melting process is modelled using a one-fluid formulation, neglecting the presence of air and is governed by the incompressible Navier–Stokes equation given by:

$$\frac{d\mathbf{u}}{dt} = -\frac{1}{\rho} \nabla P + \nabla \cdot \left( \frac{\mu}{\rho} \nabla \mathbf{u} \right) + \mathbf{f}^{\text{int}} + \mathbf{f}^B. \quad (4)$$

Here  $P$  is the pressure,  $\mu$  is the coefficient of viscosity,  $\mathbf{f}^{\text{int}}$  is the interfacial force acting at the free surface and at the liquid–solid interface and  $\mathbf{f}^B$  is the body force per unit mass acting on the fluid. The solid that undergoes melting is assumed to be rigid and interacts with the liquid domain through stresses at the interface.

The pressure is given by  $P = p + \tilde{p}$ , where  $p$  is the hydrodynamic pressure and  $\tilde{p}$  is any constant background pressure which does not contribute to the pressure gradient force due to incompressibility of the medium. The hydrodynamic pressure  $p$  is not coupled to the density and serves to ensure an incompressibility constraint such as a zero divergence velocity field

$$\nabla \cdot \mathbf{u} = 0, \quad (5)$$

or equivalently, an isochoric deformation given by a unit determinant of the deformation gradient tensor,  $\mathbf{F}$  [25]:

$$\det(\mathbf{F}) = 1. \quad (6)$$

The numerical implementation of models for heat transfer, phase change, capillary fluid flow and the solid-fluid interaction based on ISPH is explained henceforth.

### 3. SPH implementation and validation

The SPH method is based on discrete computational nodes that carry field variable values and interact with each other within a cut-off radius associated with each node. A smoothing function,  $W$  (also known as the kernel) and its derivatives are used to define continuous approximations of the field and its derivatives through convolution. Conservation of momentum is satisfied in the bulk through inter-SPH-particle forces obtained through the kernel approximations.

For an incompressible fluid, the SPH formulation for momentum conservation is [33]:

$$\begin{aligned} \frac{d\mathbf{u}}{dt}\Big|_a &= - \sum_b m_b \frac{p_a + p_b}{\rho_a \rho_b} \nabla_a W_{ab} \\ &\quad + \sum_b m_b \frac{\mu_a + \mu_b}{\rho_a \rho_b} F_{ab} \mathbf{u}_{ab} + \mathbf{f}_{ab}^{\text{int}} + \mathbf{f}_a^B, \end{aligned} \quad (7)$$

where  $m$  is the mass,  $\rho$  is the density,  $p$  is the hydrodynamic pressure,  $\mu$  is the coefficient of viscosity and  $\mathbf{u}$  is the velocity at an SPH particle  $a$  or SPH particle  $b$  in the neighborhood of  $a$ . The function  $W$  is a radially symmetric and positive definite smoothing function (also known as the smoothing kernel) with a finite cut-off radius (for the SPH discretization) defined for an SPH particle pair as  $W_{ab} = W(r_{ab}, h)$ , where  $h$  is the smoothing length of the kernel. The gradient of the smoothing function appears as  $\nabla_a W_{ab}$  for an SPH particle  $a$  with respect to its neighbor  $b$ . The radial derivative of the kernel, given by  $F_{ab}$  [21] is computed from the gradient of  $W$  as

$$F_{ab} = \frac{\mathbf{r}_{ab} \cdot \nabla_a W_{ab}}{r_{ab}^2 + \epsilon^2} \quad (8)$$

where  $\epsilon$  is a small number introduced to avoid division by zero in the rare event of SPH particles overlapping in position and is usually set to  $(0.01h)^2$ .

The hydrodynamic pressure  $p$  in incompressible flows is nothing but a Lagrange multiplier that satisfies a constraint for incompressibility given by Eq. 5 or 6. For a divergence free velocity field, following grid based fluid simulation methods, pressure is obtained by solving the pressure Poisson equation (PPE),

$$\nabla \cdot \left( \frac{1}{\rho} \nabla p \right) = \frac{\nabla \cdot \mathbf{u}}{dt}. \quad (9)$$

In the discrete SPH domain, the above equation can be approximated as

$$\sum_b \frac{m_b}{\rho_b} \frac{4(p_a - p_b)}{\rho_a + \rho_b} F_{ab} = \sum_b \frac{m_b}{\rho_b} \frac{\mathbf{u}_{ab} \cdot \nabla_a W_{ab}}{\Delta t}. \quad (10)$$

This approximation with unknown pressure values, represents a simultaneous system of linear equations in the unknowns  $p_a$ , and can be solved numerically using a linear solver such as BiCGSTAB [31]. For a domain at least partly bounded by free surfaces, a Dirichlet BC for pressure can be semi-analytically applied by the following modification to this linear system [24]:

$$(p_a - p_o)\kappa - \sum_b \frac{m_b}{\rho_b} \frac{4p_b}{\rho_a + \rho_b} F_{ab} = \sum_b \frac{m_b}{\rho_b} \left( \frac{\mathbf{u}_{ab} \cdot \nabla_a W_{ab}}{\Delta t} - \frac{4p_o}{\rho_a + \rho_b} F_{ab} \right) \quad (11)$$

where  $p_o$  represents the ambient pressure and  $\kappa$ , given by

$$\kappa = \sum_{b_{\text{bulk}}} \frac{m_b}{\rho_b} \frac{4}{\rho_a + \rho_b} \frac{\mathbf{r}_{ab} \cdot \nabla_a W_{ab}}{r_{ab}^2 + \epsilon^2}, \quad (12)$$

is a factor which remains constant for a given domain with given smoothing parameters and constant density. This modification effectively applies a penalty term that accounts for the deficiency of the kernel for an SPH particle near the free surface, and does not add to the computational cost.

Capillary forces are modelled using a pairwise SPH particle force function  $\mathbf{f}_{ab}^{\text{int}}$  based on the molecular theory of surface tension [29, 34] and is chosen to have an attractive part in the long range and a repulsive part in the short range. This capillary model is elaborated in a recent publication in the context of dynamic free surface flows [23]. We use the following pairwise force:

$$F_{\alpha\beta}^{\text{int}}(r_{ab}) = \begin{cases} -s_{\alpha\beta} \cos\left(\frac{3\pi}{4}q_{ab}\right) & q_{ab} = \frac{r_{ab}}{h'} \leq q_{\text{cutoff}} \\ 0 & q_{ab} = \frac{r_{ab}}{h'} > q_{\text{cutoff}}, \end{cases} \quad (13)$$

where  $\alpha$  and  $\beta$  represent the phases of the SPH particles  $a$  and  $b$ , respectively. The strength of the pairwise force is given by  $s_{\alpha\beta}$ . Here the cut-off distance of the pairwise force is set to be the same as that of the smoothing kernel. The strength of the pairwise force for a given macroscopic surface tension can be predetermined [34] in the presence of a free surface and this relationship is [23]:

$$\sigma = \lambda s_{ll} h_r^4, \quad \text{for 2D and} \quad (14)$$

$$\sigma = \lambda s_{ll} \frac{h_r^5}{\Delta x} \quad \text{for 3D,} \quad (15)$$

respectively. Here,  $h_r$  is the ratio of the smoothing length of the kernel to the initial SPH particle spacing  $\Delta x$  (here we use a square lattice arrangement of SPH particles as the initial condition). Note that these expressions correspond to the specific choice of pairwise force function and compact support. The constant due to integration of the pairwise force function,  $\lambda$  takes the value 0.0476 in two dimensions and  $0.0135\pi$  in three dimensions, respectively, for the interaction function given by Eq. 13 [23]. The contact angle ( $\Theta$ ) at the liquid–solid contact line is related to the pairwise force strengths [23] as

$$\cos \Theta = \frac{-s_{ll} + 2s_{ls}}{s_{ll}}, \quad (16)$$

where  $s_{ls}$  is the strength of the potential force between SPH particles belonging to the liquid and solid phase. For more information on the proper implementation of this pairwise force approach for dynamic problems, we direct the reader to [23].

We use an explicit viscous force approximation (the second term on the right hand side) that is extensively used in SPH literature [22] especially for low Reynolds number flows.

### 3.1. Heat transfer across free surface

Heat transfer problems have been solved in SPH using the approximation of second order derivatives. In finite domains, the kernel of SPH gets truncated at the interface. Our intended applications require ambient boundary conditions. This is achieved by a semi analytic Dirichlet BC for temperature similar to the application of Dirichlet pressure BC in the Laplacian of pressure presented in the previous section.

The heat transfer model (Eq. 2) is approximated in the SPH domain as follows:

$$C\rho \frac{dT}{dt} = \sum_b \frac{m_b}{\rho_b} \frac{4}{\rho_a + \rho_b} \left( \frac{k_a + k_b}{2} T_{ab} \right) F_{ab} \quad (17)$$

where,  $k_a$  and  $k_b$  represent the thermal conductivity at the SPH particle  $a$  and  $b$ , respectively and  $T_{ab} = T_a - T_b$ .

Following a similar approach to the free surface Dirichlet BC for the pressure Poisson equation [24] presented above in Eq. 11, Dirichlet boundary condition for temperature can be applied semi-analytically, as well. Applying this to the Eq. 2 leads to the following heat transfer equation approximation:

$$C\rho \frac{\partial T}{\partial t} \Big|_a = 2 \sum_b m_b \left( \frac{k_a + k_b}{\rho_a + \rho_b} (T_a - T_b) F_{ab} \right) + \kappa \frac{k_a + k_o}{2} \rho_a (T_a - T_o), \quad (18)$$

where  $\kappa$  is the same constant as in Eq. 12 and  $T_o$  is the ambient temperature (which can be time varying).

The accuracy of heat transfer is central to our problem and requires careful validation. For this, we solve the 2D heat conduction problem for a finite flat plate with two different sets of boundary conditions. In the first case in fig. (2) all four sides are modeled as free surfaces exposed to constant ambient temperature. The second setup in fig. (3) uses, aside from Dirichlet boundary conditions on three walls, an adiabatic fourth wall modeled by static SPH particles.

The heat conduction through the flat plate across the free surface is compared to the analytical solution at different times in Fig. 2 where the plate is heated at constant temperature from the ambience on all four sides. An array of  $160 \times 160$  fixed SPH particles are used to represent a square flat plate of side  $l = 0.1$  m. The ambient temperature is set to 0 K and the plate is set to a uniform initial temperature of 1 K. Throughout this paper, when no material property is dependent on temperature, only the gradient of temperature appears in the governing equations for heat transfer. Hence the temperature and the corresponding conditions for the phase change region can be shifted by an additive constant. Hence the use of 0 K here does not suggest the thermodynamic absolute zero. The density of the material is set to  $1 \text{ kg m}^{-3}$  and the thermal diffusivity is set to  $1 \times 10^{-4} \text{ m}^2 \text{s}^{-1}$ .

In Fig. 3, an adiabatic wall with a homogeneous Neumann BC for temperature is applied. The simulation results are compared to analytical solutions, available widely in standard text books on numerical methods [16], and a very good match is observed.

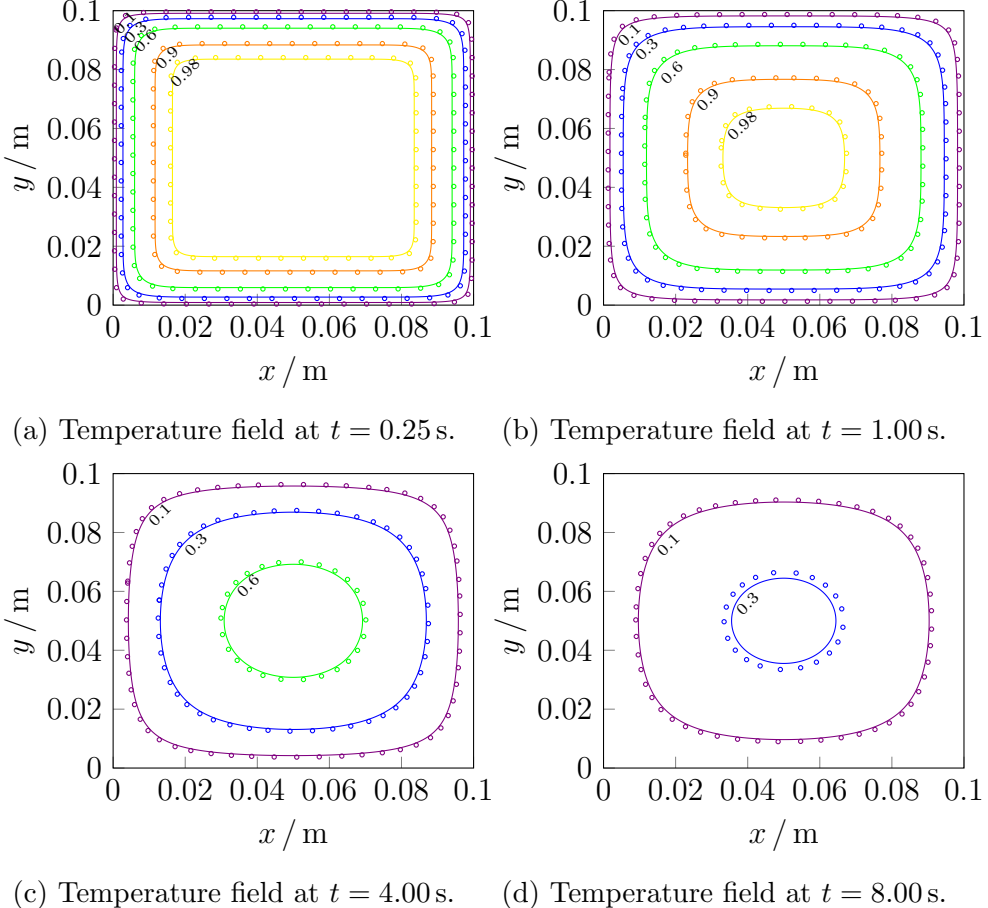


Figure 2: Evolution of the temperature profile within a square at different times for a resolution of  $160 \times 160$  SPH particles with Dirichlet BC on all sides.

The consistency of this heat transfer model can be seen in Fig. 4, showing greater than first order accuracy. The  $L_2$  norm of the error at different times are presented against the resolution of the domain. The order of accuracy of the heat transfer simulation with the free surface BC can be clearly seen to be more than first order in Fig. 4.

### 3.2. Static phase change

Phase change is modelled using the effective heat capacity  $C_{\text{eff}}$  defined in Eq. 3. There are different strategies for implementing the effect of latent heat into a numerical method. On the one hand it can be added as a source term to the heat conduction equation [37, 26] or, on the other hand, by modifying the heat capacity itself [8, 35, 13]. In this work an integral interpolation introduced by [8] is implemented to modify the heat capacity in order to model phase change processes. Therefore, the model for a smoothed latent heat in SPH can be derived by starting from the definition of an effective heat capacity  $C_{\text{eff}}$  which includes the effect of latent heat [4, 14] given by Eq. 3. This formulation is composed of the heat capacities for solid  $C_s$  and  $C_l$  liquid phase as well as the heat capacity within the phase change region  $C_m$ . Here,  $C_{\text{eff}}$  at the melting temperature  $T_m$  includes the total latent heat

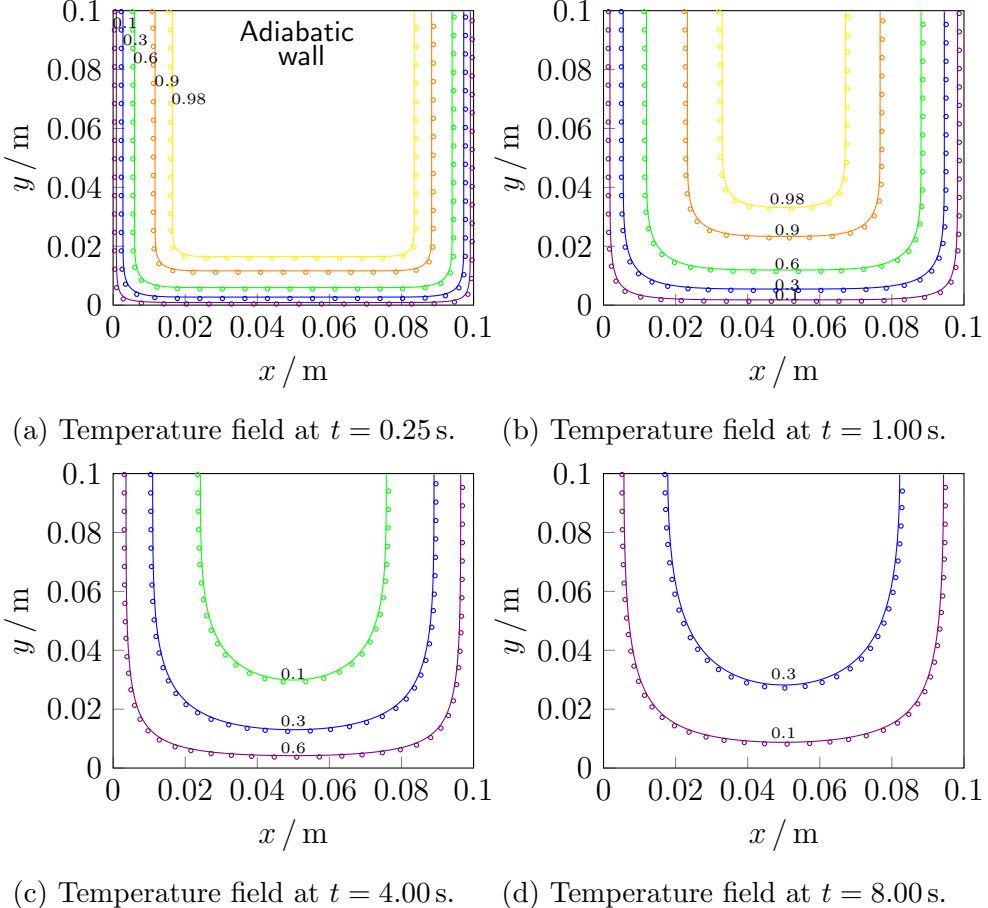


Figure 3: Evolution of the temperature profile within a square at different times for a resolution of  $160 \times 160$  SPH particles with Dirichlet BC on three sides and Neumann on the fourth.

of the phase change,  $L = \int_{-\infty}^{\infty} L\delta(T - T_m)$ .

The Dirac function can be replaced in the one-dimensional temperature domain by a kernel function  $W_T$  with smoothing length  $h_T$  analogous to the spatial kernel function in SPH resulting in:

$$C_{\text{eff}} = \begin{cases} C_s & T < T_m - \Delta T \\ C_m + LW_T(T - T_m, h_T) & T_m - \Delta T \leq T \leq T_m + \Delta T \\ C_l & T > T_m + \Delta T \end{cases} \quad (19)$$

The temperature domain  $\Delta T$  represents a mushy region around the phase change temperature. The size of this region is defined as the product of the smoothing length  $h_T$  and the maximum range of support  $q_{\max}$  of the temperature kernel.

$$\Delta T = h_T q_{\max}. \quad (20)$$

The outcome of this is a changing  $C_{\text{eff}}$  inside of this region with a maximum latent heat effect at the phase change temperature. The accuracy of this approach is further improved

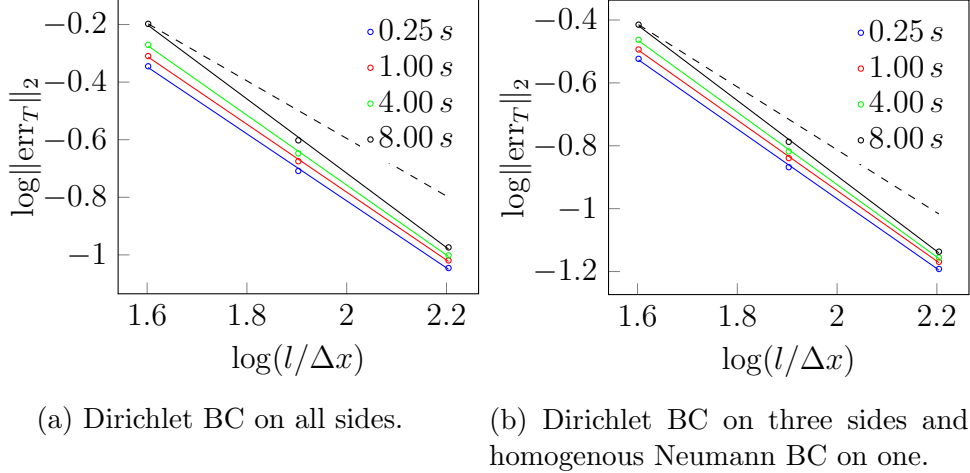


Figure 4:  $L_2$  norm of the error in temperature ( $T$ ) in the domain at different times and spatial resolutions. The plot shows the order of accuracy greater than 1 at all time instances. Dashed lines in both the plots indicate first order convergence, provided for reference.

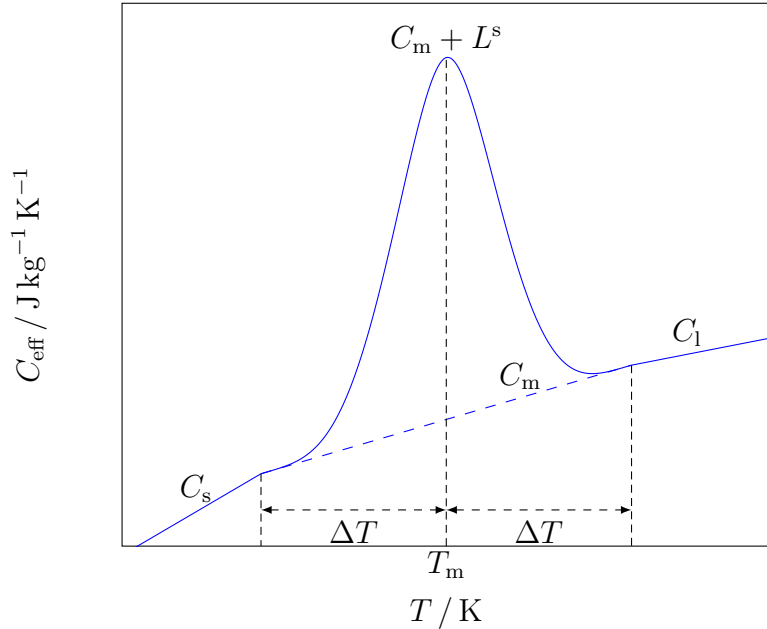


Figure 5: Smoothed effective heat capacity within the mushy region of the phase transition temperature. The increase in specific heat at the interface is  $L^s = LW_T(T - T_m, h_T)$  in the mushy region.

by considering the distance between adjacent SPH particles and the temperature difference with respect to the transition temperature. This results in a smoothed latent heat  $L^s$  [8] for a SPH particle  $a$  defined as

$$L_a^s = \sum_b \frac{m_b}{\rho_b} (LW_T(T_b - T_m, h_T)) W(\mathbf{r}_b - \mathbf{r}_a, h). \quad (21)$$

This results in the effective heat capacity given in equation (22) which is replacing the

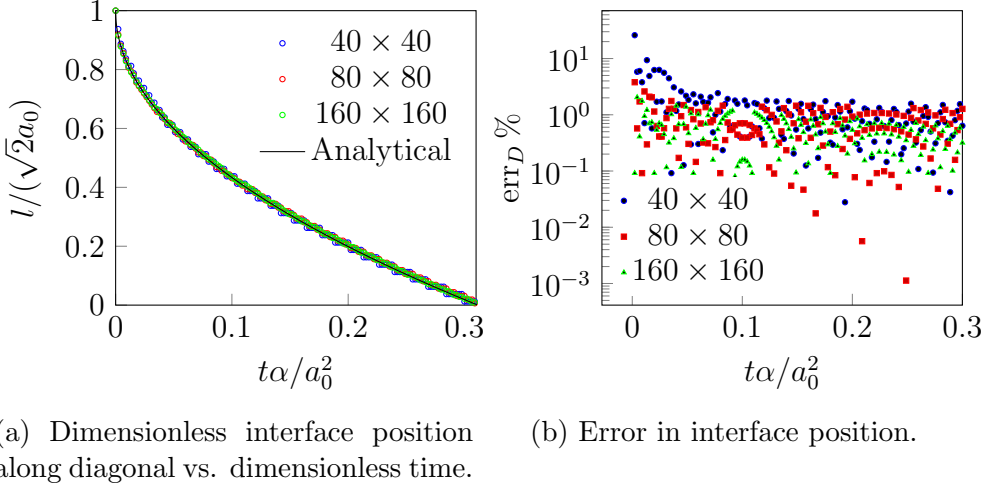


Figure 6: Neumann problem: Interface position (a) and calculated errors (b) obtained for different resolutions. The characteristic length  $a_0$  is the side of the quarter of the square plate undergoing phase change.

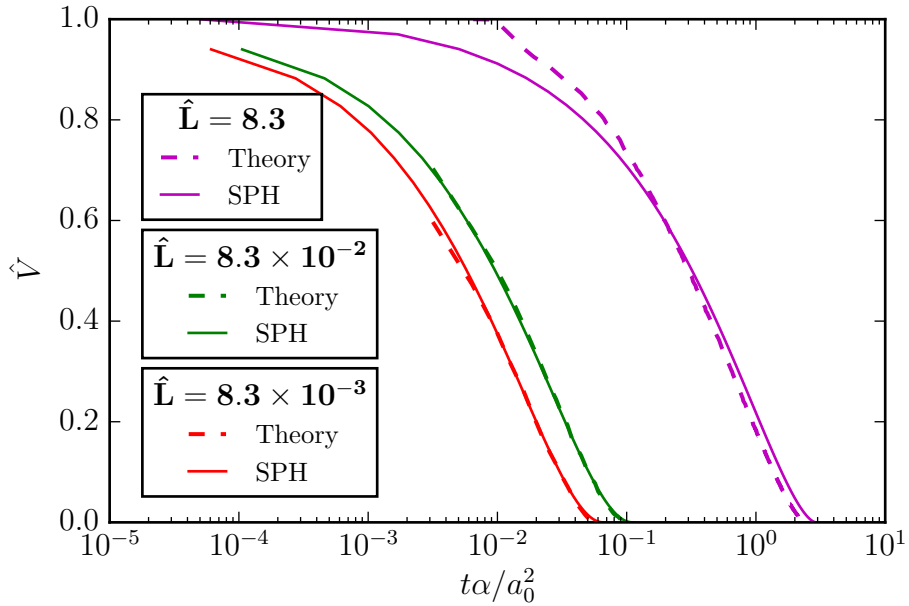


Figure 7: Static melting of a spherical solid—comparison of evolution of solid volume fraction with 1D axisymmetric theory. Here  $\hat{L}$  is the non-dimensionalized latent heat,  $\hat{L} = L / (k_s(T_o - T_m))$ .

specific heat capacity of the heat conduction equation (17).

$$C_{\text{eff}} = \begin{cases} C_s & T < T_m - \Delta T \\ C_m + L^s & T_m - \Delta T \leq T \leq T_m + \Delta T \\ C_l & T > T_m + \Delta T \end{cases} \quad (22)$$

The effective heat capacity augmented by the smoothed latent heat is shown in Fig. 5.

The phase change model in SPH together with the free surface BC for ambient temperature needs to be validated. Here we choose the Neumann problem in 2D [27] and the Stefan's problem in axisymmetric 3D [19] to validate the evolution of the melting interface with time.

In two dimensions, the two edges of a right angled corner of a 2D square plate is heated. The medium is set to a density of  $1 \text{ kg/m}^3$ . The initial and melting temperature are set to 2.0 and 2.3 K respectively. The thermal conductivity and specific heat capacity of both phases were maintained at a value of 1 in SI units. The latent heat was set to 0.25 J/kg. Three different resolutions were considered corresponding to 40, 80 and 160 SPH particles along one direction in the quarter space of dimensions  $a = 3 \text{ m}$ . The choice of these parameters are arbitrary, since the aim of the validation is only to check the numerical approximation of the model. In the following section we will resort to more realistic simulation parameters. As the temperature rises above the melting temperature, the solid melts and the solid–liquid interface moves inwards. The location of the phase change interface along the diagonal, normalized by the width of the plate is plotted against non-dimensional time in Fig. 6a. The melting process is assumed to be static, such that the molten region is assumed to not deform. This problem is simulated without liquid deformation for different spatial resolutions and compared against the analytical solution. Note that the heat transfer across the free boundary is based on the semi-analytic boundary formulation in Eq. 11. The interface location appears as a stepped curve because of the discrete sampling in time. We see that the interface evolution is predicted accurately. In Fig. 6b we see the order of accuracy increases with increasing resolution, consistently. The discrete sampling in time makes it difficult to obtain the exact order of accuracy.

In 3D, we solve the Stefan's problem in a sphere and compare the results with the solutions of an axisymmetric model proposed in [19], given by

$$\frac{\partial h}{\partial \hat{t}} = \frac{\partial^2 \hat{T}}{\partial r^2} + \frac{2}{r} \frac{\partial \hat{T}}{\partial r} \quad \text{in } 0 < r < 1, \quad (23)$$

where  $r$  is the radial location in the unit sphere, normalized by the radius of the sphere,  $R$ . Time is normalized by  $R^2/k_s$ , where  $k_s$  is the thermal conductivity of the solid phase. The enthalpy  $H$  is related to the temperature  $\hat{T}$  (normalized by  $(T_o - T_m)$ ) by

$$\hat{T} = \begin{cases} H - \beta, & H < 0 \\ 0, & 0 \leq H \leq \beta, \\ \tilde{k}(H - \beta), & H > \beta, \end{cases} \quad (24)$$

where  $\beta$ , the Stefan number is given by  $\beta = L/(C_s(T_o - T_m))$ , where  $C_s$  is the specific heat capacity of the solid phase. Also  $\tilde{k}$  represents the ratio of thermal diffusivities of the solid and liquid phases respectively,  $\tilde{k} = k_l/k_s$ . Eq. 23 is solved using finite difference method as given in [19] and [36]. We discretized the spatial derivatives using a central difference approximation and the temporal derivatives using forward time Euler approximation and solved the system explicitly to obtain the melting interface position in time.

In order to motivate application to realistic materials, we present the results for different latent heat spanning different orders of magnitude. Though the results presented are non-dimensionalized, the material parameters are chosen to resemble realistic materials and these

parameters will be used for further simulations in the dynamic context in the next section. In Fig. 7 we present the time evolution of the volume of the solid,  $\hat{V}$ , during melting. Instead of the location of the interface position, we present the volume of the solid remaining at different instances in time. Since our goal is to present the effect of shape of the melting body, we choose the volume of the solid instead of a linear dimension. The simulation and discretization parameters are presented in Table 1. Three different latent heat values are considered.

We see that for lower latent heat values, the match is accurate. However, for large latent heat values, the onset of melting is slightly different from the analytic solution. This is perhaps due to the truncated temperature and spatial kernel used in computing the latent heat. We will be addressing this in a future work.

Quantity	Value	Unit
$\sigma$	0.2308	Nm <sup>-1</sup>
$\Theta$	30	°
$\mu$	0.001793	Pas
$\rho$	1000	kg m <sup>-3</sup>
$T_{\text{initial}}$	1	K
$T_m$	1.15	K
$T_o$	4.0	K
$C$	2.11	kJ kg <sup>-1</sup> K <sup>-1</sup>
$L$	0.1, 1.0, 100.0	kJ kg <sup>-1</sup>
$k_s, k_l$	2.14	W m <sup>-1</sup> K <sup>-1</sup>
$\Delta x$	$4.0 \times 10^{-5}$	m
$\Delta T$	0.1	K
$R$	$5.66 \times 10^{-4}$	m

Table 1: Parameters used to simulate melting of a sphere and a mill particle.

The time update is numerically stable only when  $\Delta t$  satisfies the condition

$$\Delta t \leq \min_a \left( 0.25 \frac{h}{3|\mathbf{u}_a|}, 0.25 \sqrt{\frac{m_a h}{3|\mathbf{f}_a^{\text{int}}|}}, 0.25 \frac{\rho h^2}{9\mu} \right). \quad (25)$$

#### 4. Applications: Melting dynamics

The multiphysics SPH algorithm is implemented in an ISPH code [24, 25] and melting problems with flow dynamics are solved for complex shaped three dimensional solids. Results are compared with theoretical results and other numerical studies with simplistic assumptions.

##### 4.1. Melting of a mill particle

A complex shaped geometry obtained by scanning a mill particle from an industrial process is shown in Fig. 8. This geometry is filled with SPH particles in a square lattice

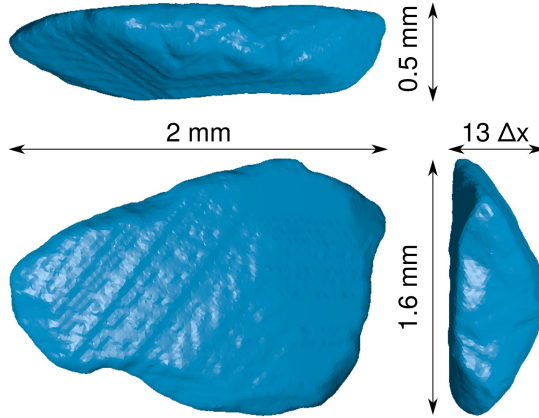


Figure 8: Dimensions of the complex shaped mill particle in mm. The initial discretization length between SPH particles is given by  $\Delta x$ .

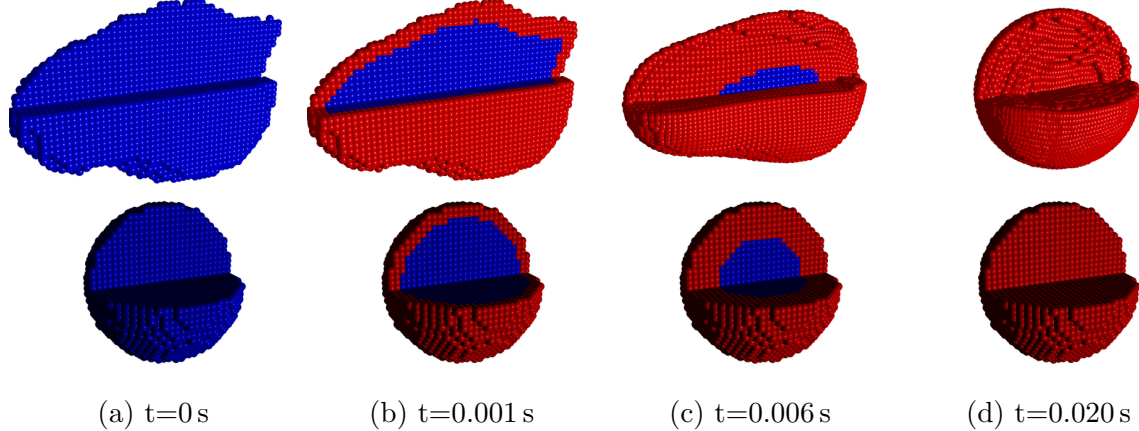


Figure 9:  $L = 0.01 \text{ kJ/kg}$ : Melting of an irregular shaped mill particle vs. a static sphere. Blue colored SPH particles denote solid and red colored SPH particles denote liquid phase.

with the same initial spacing and simulation parameters as that used in the melting of spheres presented in the previous section. Figure 8 also shows the dimensions of the particle and the SPH intial particle resolution for simulation in the smallest dimension ( $\Delta x = 0.04 \text{ mm}$ ). The volume of the mill particle is chosen to be equal to the volume of the sphere in the previous section. We have avoided discontinuities in the thermal properties across the solid–liquid interface in order to compare with the theoretical results and to focus on the melting and capillary force based deformation as the first step. Discontinuities in the thermal properties will be introduced in the subsequent applications (Sec. 4.2) of the method.

The evolution of the solid and liquid phases are shown in Figs. 9–14. Since different physical processes are coupled in this simulation, we have not attempted to non-dimensionalize this system. However, the rate of phase change is non-dimensionalized in order to be compared with the melting of the sphere in the previous section.

In Figs. 9 and 10 blue and red SPH particles represent solid and liquid phases, respec-

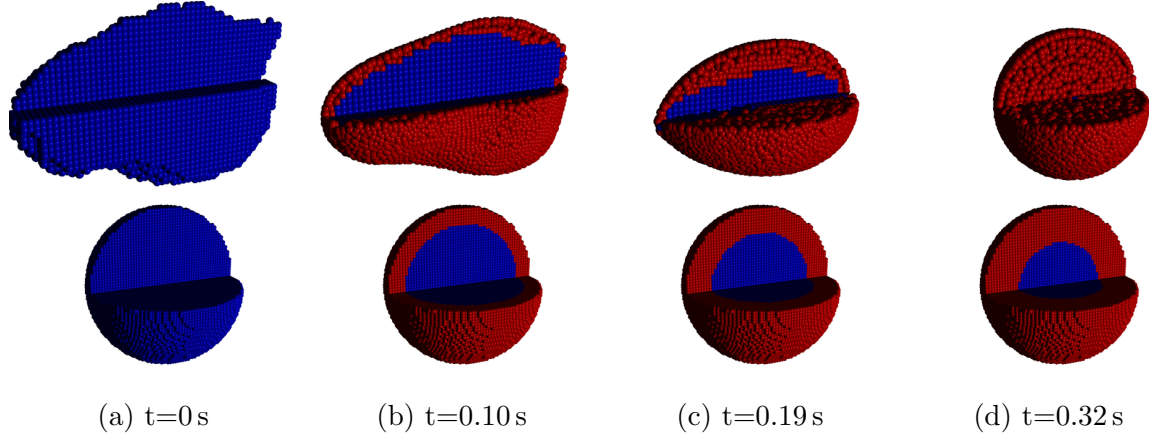


Figure 10:  $L = 100.0 \text{ kJ/kg}$ : Melting of an irregular shaped mill particle vs. a static sphere. Blue colored SPH particles denote solid and red colored SPH particles denote liquid state.

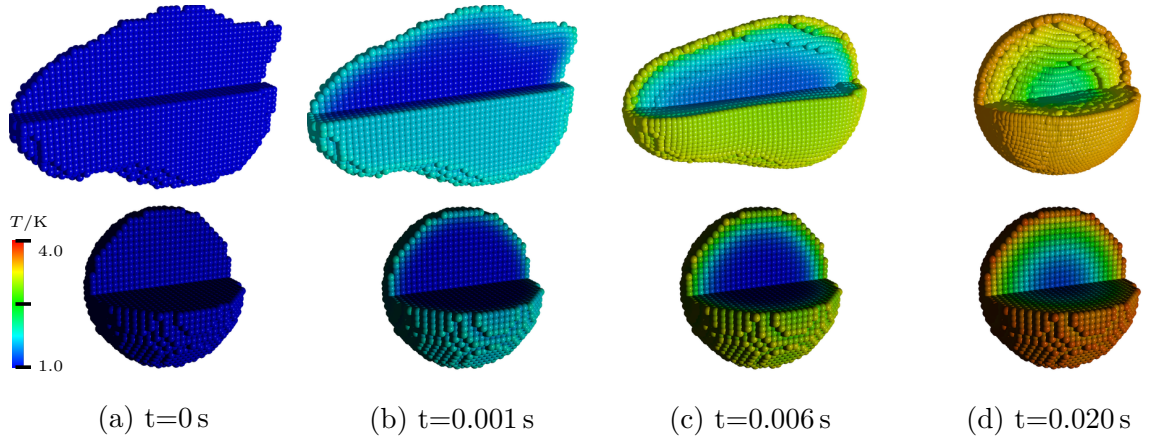


Figure 11:  $L = 0.01 \text{ kJ/kg}$ : Temperature profile in the melting mill particle.

tively. For better illustration, a quadrant is clipped out of the irregular particle to show the scalar field evolution in the bulk of the particle. At the beginning of the simulation, all SPH particles are in solid state. As a result of the heating from the constant ambient temperature, the phase change occurs as the temperature rises above the melting point. A layer with liquid SPH particles are formed at the surface of the mill particle after about 0.001 s for the latent heat of 0.01 kJ/kg and 0.10 s for the latent heat of 100 kJ/kg. The liquid–solid interface is hydrophilic owing to the acute contact angle of 30°. The contact angle due to homologous wetting between a molten metal and its solid counterpart is often assumed to be a function of the Stefan number [6], and can be a complex property to determine. We have therefore used an arbitrary hydrophilic contact angle in our simulations. Hence the unmelted solid remains wetted by the melt. Since the melting is slower for higher latent heat, the fluid relaxes more and this can be seen at 0.19 s in the large latent heat case, where the liquid has assumed a shape close to a prolate ellipsoid. For both the latent heat values considered, the surface roughness (resolved by the initial SPH particle resolution) smoothes

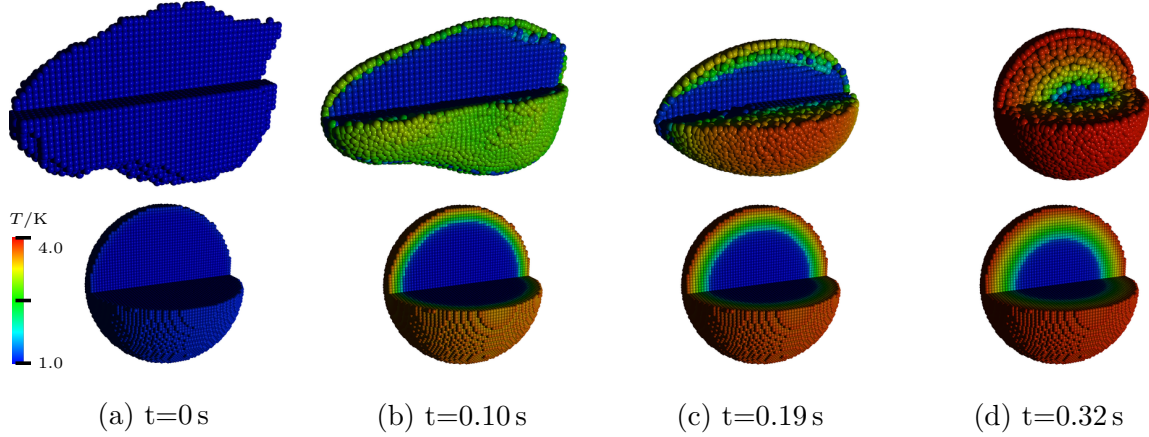


Figure 12:  $L = 100.0 \text{ kJ/kg}$ : Temperature field in the melting particles. Top row shows the mill particle with melt flow and the bottom row shows a static spherical particle.

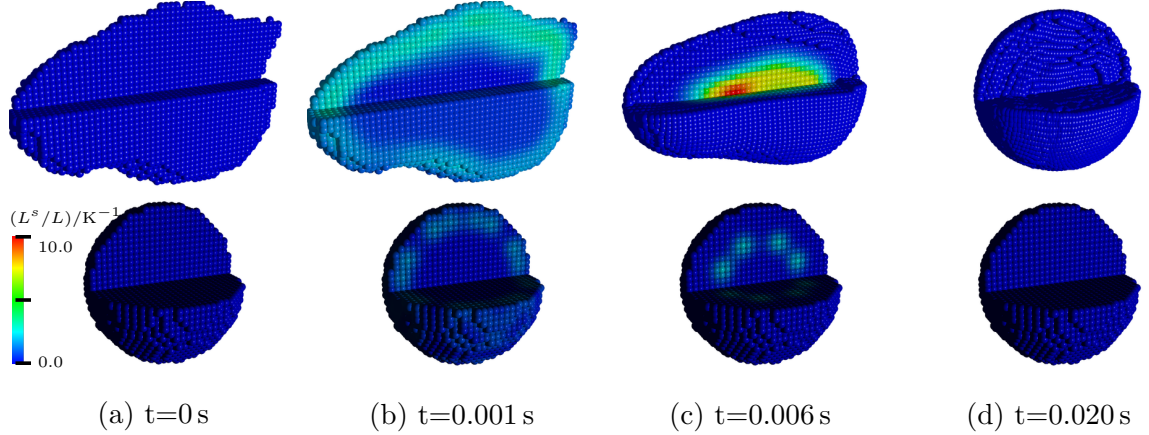


Figure 13:  $L = 0.01 \text{ kJ/kg}$ : Increase in heat capacity at the interface during the melting of the mill particle.

out differently, since the melting rate is faster than the capillary relaxation process for low latent heat value. Also, for low latent heat, the particle rounding takes place much later than the complete melting of the solid. Once it achieves the spherical shape the melt drop oscillates about its mean spherical shape. Such oscillation of a viscous fluid drop using the same pairwise force capillary model is validated against analytical results in [23].

In Figs. 11 and 12, the temperature field of the melting body is shown at different instances. With the onset of heat exchange with the ambiance the solid phase SPH particles start to heat up from the free surface. When the first layer of liquid SPH particles is formed (at  $0.001\text{ s}$  for  $L = 0.01 \text{ kJ/kg}$  and at  $0.10\text{ s}$  for  $L = 100 \text{ kJ/kg}$  ) the temperature gradient normal to the solid surface is much larger for the larger latent heat case.

A layer of SPH particles on the free surface change to liquid as they attain the melting temperature uniformly and covers the solid particle. Due to capillary relaxation the liquid SPH particles near the free surface flow to the vicinity of the solid body, where they cool down. It is also possible that colder liquid SPH particles are transported back to the surface

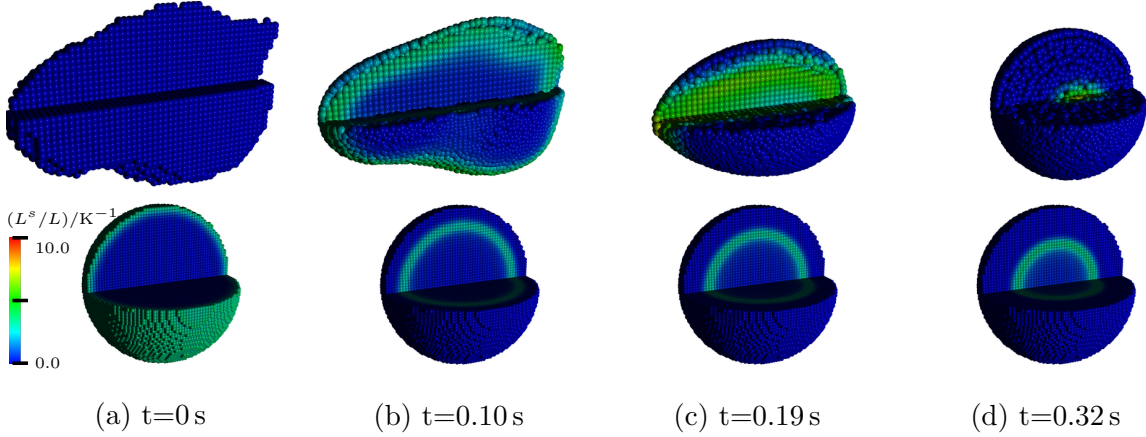


Figure 14:  $L = 100.0 \text{ kJ/kg}$ : Increase in heat capacity at the interface during the melting of the mill particle.

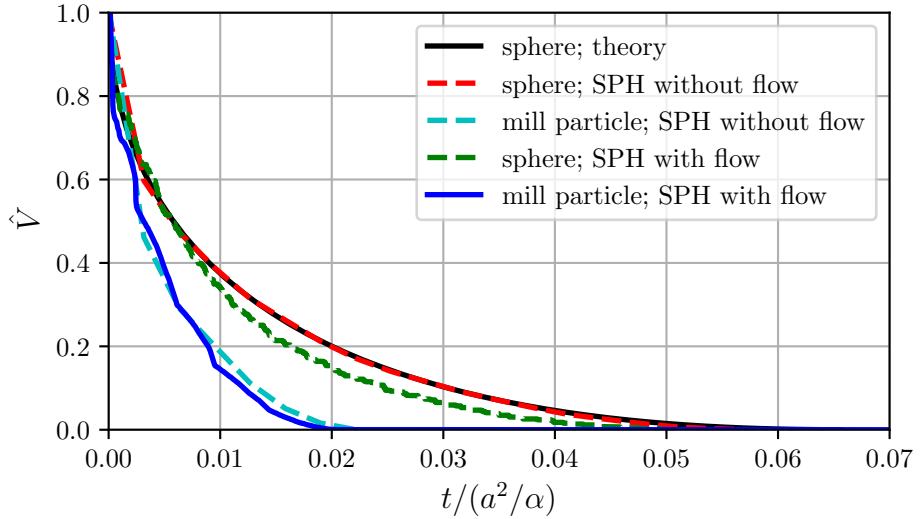


Figure 15:  $L = 0.01 \text{ kJ/kg}$ : Time variation of volume fraction of solid for a sphere and the mill particle of equal volume.

where they are heated up. This convective heat transfer is evident in the case of mill particle and is absent in the case of the static sphere. This can be clearly seen in Fig. 10d, where the mill particle melts much faster than the compared static sphere, where capillary relaxation isn't playing any role and the surface area to volume ratio is much smaller. In Figs. 13 and 14, the regions where latent heat is effective are shown. As the temperature rises, SPH particles enter the mushy region (Eq. 21), where the latent heat integrated over the mushy temperature range ( $T_m - \Delta T < T < T + \Delta T_m$ ) is shown. From Figs. 13c and 14c, we see that the latent heat distribution near the interface is rather uniform.

To appreciate the effect of shape of the particle and its latent heat on the melting rate, the evolution of solid fraction of the unmelted solid are shown in Figs. 15, 16 and 17. In

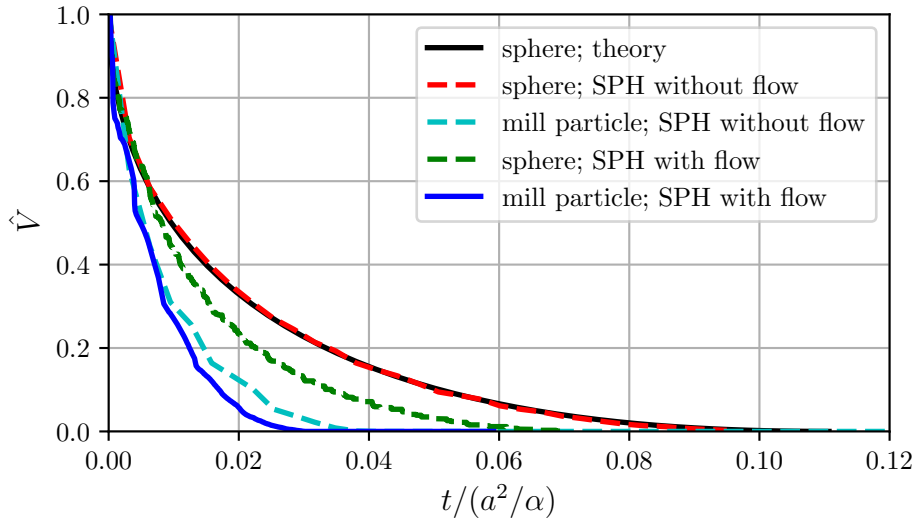


Figure 16:  $L = 0.1 \text{ kJ/kg}$ : Time variation of volume fraction of solid for a sphere and the mill particle of equal volume.

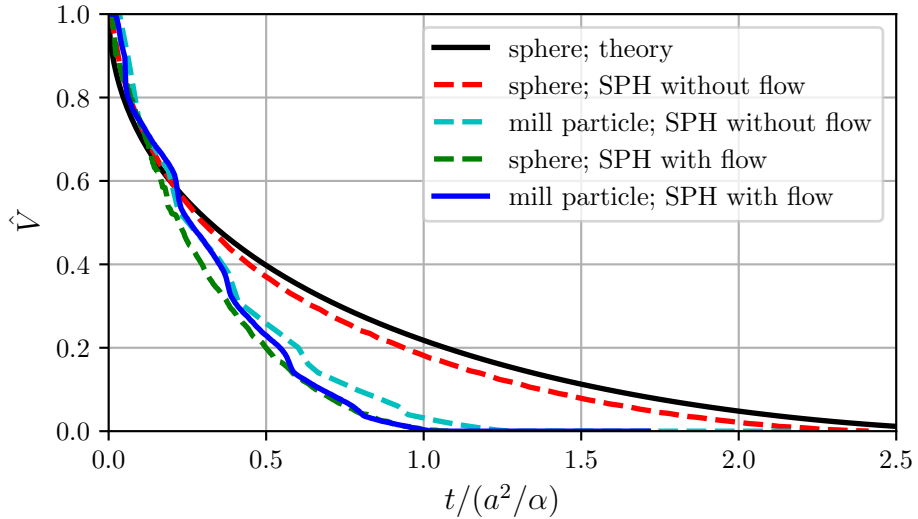


Figure 17:  $L = 100 \text{ kJ/kg}$ : Time variation of volume fraction of solid for a sphere and the mill particle of equal volume.

each of the three plots, a sphere with no melt flow (static melting), a sphere with melt flow (dynamic melting), the mill particle with no flow and the mill particle with melt flow are simulated. The axisymmetric theoretical result for each of these latent heat values [19] is shown by solid black lines and are essentially the same as in Fig. 7. For a low latent heat of  $0.01 \text{ kJ/kg}$ , the static and dynamic melting of the sphere evolves closely and is considerably different from those for the melting of the mill particle. The surface area of the mill particle

is 1.4 times that of the sphere of the same volume. The effect of the larger surface area reflects in the rate of melting of the mill particle. Since the capillary relaxation drives the flow in the arbitrary shaped mill particle, convection heat transfer also influences the melting process. Though the static melting compares well with the theoretical result, the dynamic melting of sphere deviates slightly from this melting rate. This could be because of flow related to the capillary relaxation due to noise in the simulation. One reason for this noise could be the spurious currents generated from the initial approximately spherical shape of the liquid layer. The spurious currents in initially spherical shapes in all numerical methods warrants separate attention [3]. In realistic scenarios, however, there could be noise that causes convective heat transfer even within a spherical drop of liquid due to other causes such as buoyancy and Gibbs-Marangoni effects. Convection in the dynamic sphere case is even more evident as the latent heat increases as seen in Figs. 16 and 17, the latter case where the dynamically melting sphere is closer to the melting evolution of the mill particle than the static case. Notwithstanding, the effect of shape (surface area) is evident from these plots. For the large latent heat case (Fig. 17 and 16), the mill particle (with and without flow) melts at a considerably faster rate than the static sphere. However the effect of convection due to flow in the mill particle causes difference in rate of melting between the mill particle with and without flow. The time for capillary relaxation compared to the time scale of phase change rate (which is dependent on the latent heat) is also the reason for increased convective heat transfer in the melt.

#### 4.2. Agglomeration of a chain of melting solids

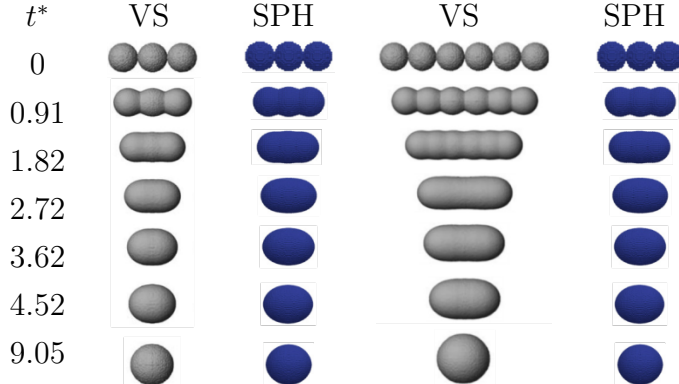


Figure 18: Shape evolution of agglomerate chains with three and six spheres. On the left side of each subfigure are the viscous flow sintering (VS) solutions by [15]. The right hand side of each of the case is the SPH simulation using only viscous flow assumption.

In order to motivate the application of the proposed SPH approach to understand the structural evolution of melting solids with realistic transport and thermal properties, we present the simulation of agglomeration of melting spheres. Such agglomeration is sometimes approximated as a slow viscous flow sintering phenomenon [15] in the low Reynolds number regime. In such an assumption, which is indeed valid for many engineering applications, a

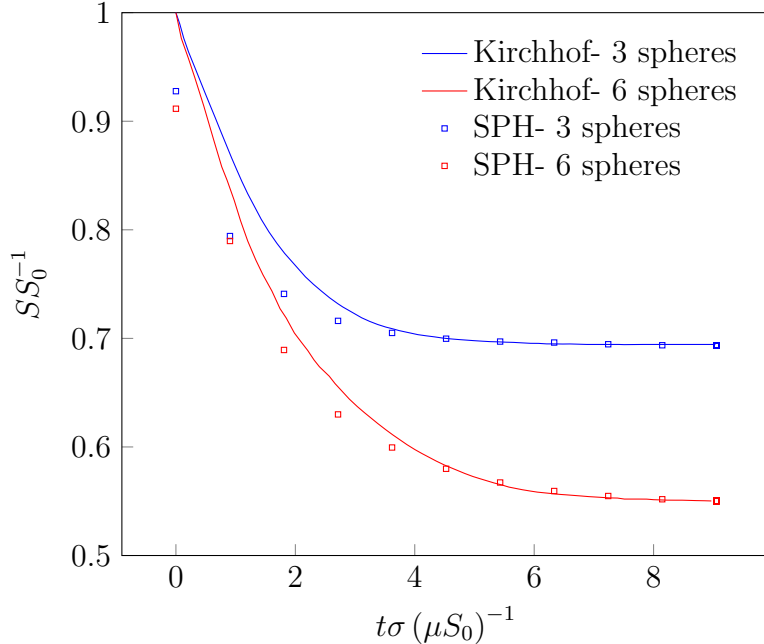


Figure 19: Dimensionless surface area evolution of agglomerate chains with three and six spheres. The surface area is normalized with the initial surface area  $S_0$  of the primary particles. The normalized surface area determined by [15] are given as solid lines whereas the SPH viscous flow simulation results are shown as hollow circles.

non dimensional time can be defined as [15]

$$t^* = \frac{t\sigma}{\mu r_0}, \quad (26)$$

where  $\sigma$  is the surface tension,  $\mu$  is the dynamic viscosity,  $r_0$  is the radius of one primary sphere and  $t$  is the time. However, when the melt flow dynamics and heat transfer is fully coupled, the resulting structural change cannot be represented by a single non dimensional quantity. Hence we proceed to show the deviation of the surface evolution of melting solids from that of the viscous flow sintering assumption.

Initially, we perform 3D simulations of viscous flow sintering similar to that given in [15], using only viscous flow assumption in SPH and compare these results in Fig. 18 for both. A very good visual agreement is observed. Further, in Fig. 19, the evolution of dimensionless surface area of the agglomerate spheres is compared with the viscous sintering simulations and the quantitative agreement is clearly seen. We now simulate the spheres as solids with a finite latent heat, undergoing melting due to the heat transfer from ambience, through conduction and subsequent convection during flow of the melt. In table 2, we present the transport and thermal properties of the materials we simulate. Compared to the previous study of rounding of the mill particle, we have introduced discontinuities in the thermal properties between the solid and liquid phases in this case.

We present the melting dynamics of 3 spheres with a latent heat value of 100 kJ/kg. The phase, temperature and local latent heat are presented in Figs. 20, 21 and 22 respectively at

Table 2: Thermodynamic properties of the solid and liquid SPH particles as well as the ambient pseudoparticles for the melting of an agglomerate chain with three primary spheres.

Quantity	Value	Unit
$\sigma$	$7.12 \cdot 10^{-2}$	N m <sup>-1</sup>
$\Theta$	30.00	°
$\mu$	$1.00 \cdot 10^{-3}$	Pa s
$\rho$	$1.00 \cdot 10^3$	kg m <sup>-3</sup>
$T_0$	1.00	K
$T_m$	1.15	K
$k_s$	2.14	W m <sup>-1</sup> K <sup>-1</sup>
$k_l$	0.56	W m <sup>-1</sup> K <sup>-1</sup>
$C_s$	$2.11 \cdot 10^3$	J kg <sup>-1</sup> K <sup>-1</sup>
$C_l$	$4.22 \cdot 10^3$	J kg <sup>-1</sup> K <sup>-1</sup>
$L$	1.00	J kg <sup>-1</sup>
$T_{\text{amb}}$	4.00	K
$k_{\text{amb}}$	0.56	W m <sup>-1</sup> K <sup>-1</sup>
$c_{p, \text{amb}}$	$4.22 \cdot 10^3$	J kg <sup>-1</sup> K <sup>-1</sup>

different time instances. After 0.0025 s, a thin layer of liquid is formed on the spheres, which coalesce with the adjacent spheres. The resulting fluid-solid interaction results in a complex free surface evolution, remarkably different from the assumption of viscous flow sintering in Fig. 18. Up to 0.0089 s, the overall shape remains rather symmetric. A marked instability is observed at 0.0521 s as the numerical errors serve as perturbation, resulting in a sudden decrease in surface area. From this point, the overall shape remains a sphere even though the solids have not all melted. At 0.1341 s, two out of the three primary spheres are completely molten, implying that the non-linear motion of the spheres also affect heat transfer in the bulk of the material. This clearly shows that the presence of yet to melt solids as suspensions influencing the shape evolution of the melt itself.

In order to appreciate the influence of the fluid–solid interaction and the capillary viscous flow on the shape evolution, we present two simulations with varying thermal and transport properties resulting in shape evolution in comparable time instances, in Fig. 23. These properties are chosen in such a way that the shape evolves into a sphere in approximately same time scales. Multiphysics simulation shown on the right column of this figure uses a viscosity coefficient that is 1000 times smaller than the viscosity used in the viscous flow sintering simulation shown on the left column. Meanwhile, a realistic latent heat value of 100 kJ/kg is used for multiphysics simulation in the right column to slow down the phase change and thereby the rounding process. At these values, the shapes evolve at comparable rates as seen in Fig. 23. Since the fluid is not all molten for the given time instances, the fluid-solid interaction results in complex shapes, often resulting in low aspect ratio shapes compared to the result from the linear assumptions. In microstructure evolution in additive manufacturing, including the influence of such fluid-solid interaction would provide insight into the melt flow, pore evolution, defect formations and also in determining optimal layer thickness during the powder spreading processes.

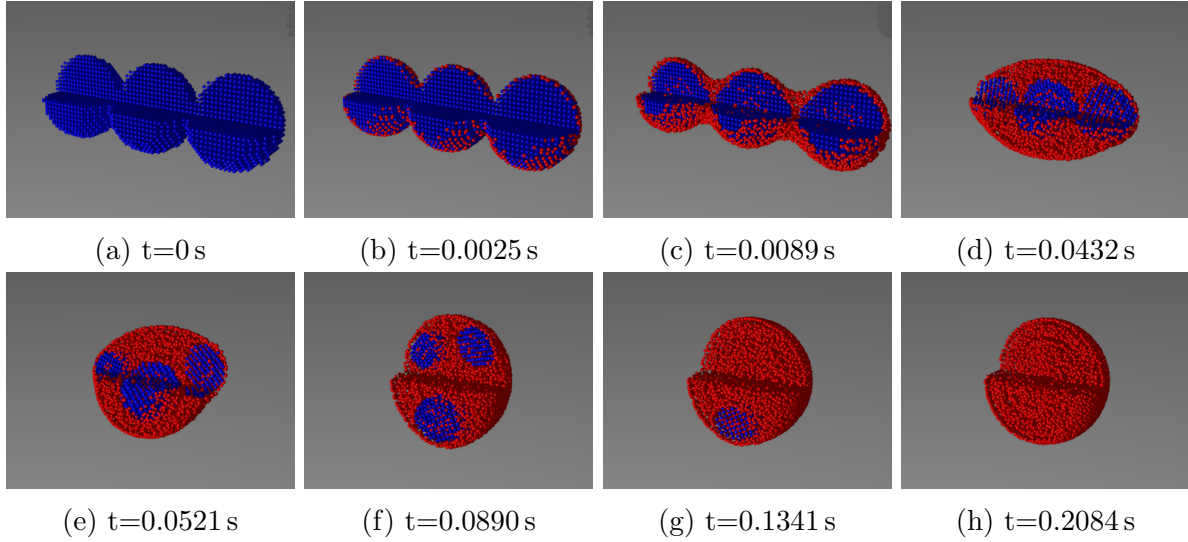


Figure 20: Representation of the solid-liquid phase change of an agglomerate chain with three primary particles. Blue colored SPH particles denote solid and red colored SPH particles liquid state. Melting occurs until all SPH particles are in the liquid state and form a sphere.

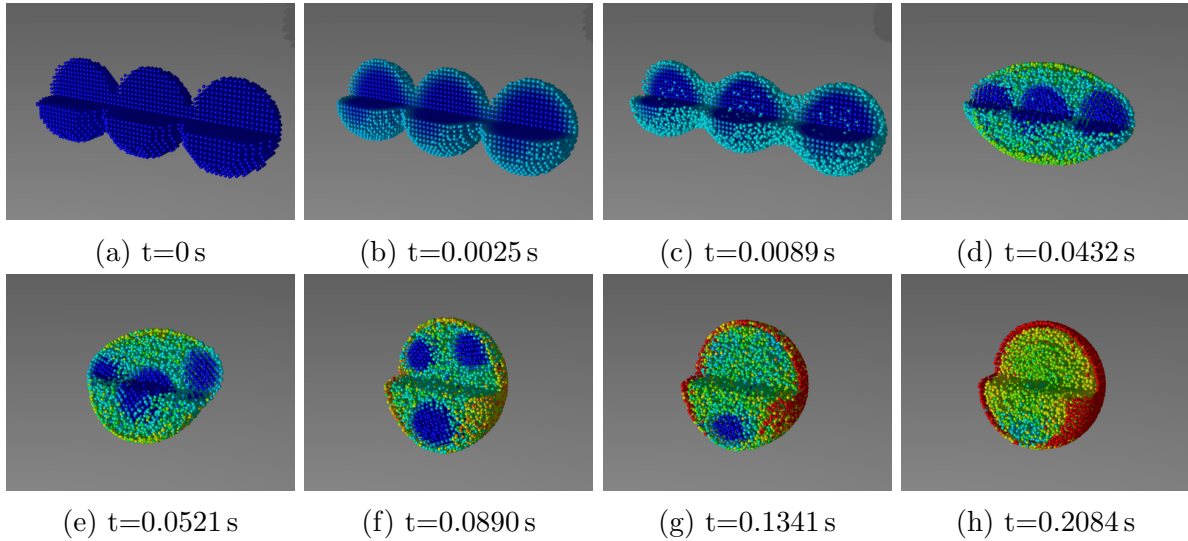


Figure 21: Temperature profile of three primary particles forming an agglomerate chain and liquid state particles formed during the melting process. The temperature takes values between 1.0 K (blue colored) and 3.034 K (red colored).

## 5. Conclusions

A multiphysics SPH method that couples heat transfer, phase change and capillary flow solver is presented in the context of Incompressible Smoothed Particle Hydrodynamics. A constant volume melting model is implemented. The melting model is based on a specific heat capacity that increases additively by the latent heat of the material, near the melting interface and at temperatures close to the melting point. Heat transfer across the free

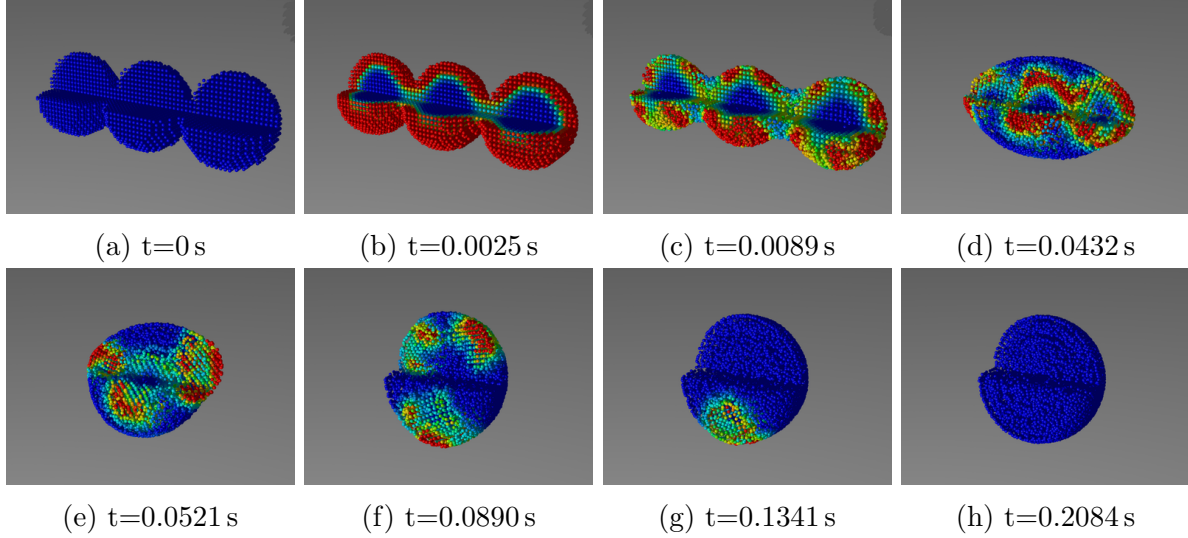


Figure 22: Representation of the regions in which the SPH particles are located in the temperature range of the phase change. The effect of latent heat is normalized and has its greatest effect in red-colored areas. Blue colored SPH particles are outside the mushy-region for the phase change and experience no effect due to the latent heat.

surface through a semi-analytic Dirichlet BC across the free surface allows the simulation of complex shaped bodies. The method is carefully validated against theoretical models on melting and conduction heat transfer. leads to spurious velocities increasing the convective thermal transport compared to theory.

The method is first applied to study the influence of particle shape on its surface evolution during heating and subsequent melting of the particle. We simulate melting process across a range of latent heat values and show that at high latent heat values the melting process evolves substantially differently from assumptions of a spherical shape. A non spherical shape, owing to its increased surface area melts faster than a sphere of the same volume. Additionally, capillary flow of the melt further increases the heat transfer due to the flow within the melt and accelerates the melting process. However the influence of spurious currents, typical of numerical capillary flow simulations, is also seen in the simulations of melting spheres. This persistent issue requires further detailed attention.

The method is then applied to the study of agglomeration of a chain of particles that undergo melting. The results are compared against simulations that assume viscous flow sintering. We show that when unmelted solid particles are present (owing to large latent heat of melting of the material), the evolution of shape of the agglomerate follows a highly non-linear path due to the fluid–solid interaction within the body of the melt. Thus, a case is made for the method’s applicability to microstructure studies in additive manufacturing where time scales of the flow and phase change are comparable.

Additional effects such as Marangoni forces and recoil pressure (in case of metals) also play an important role in additive manufacturing. Modeling of these phenomena in the context of SPH and their compounded effect on the dynamics of melting require elaborate study. In this work, we have used representative transport and thermal properties. However

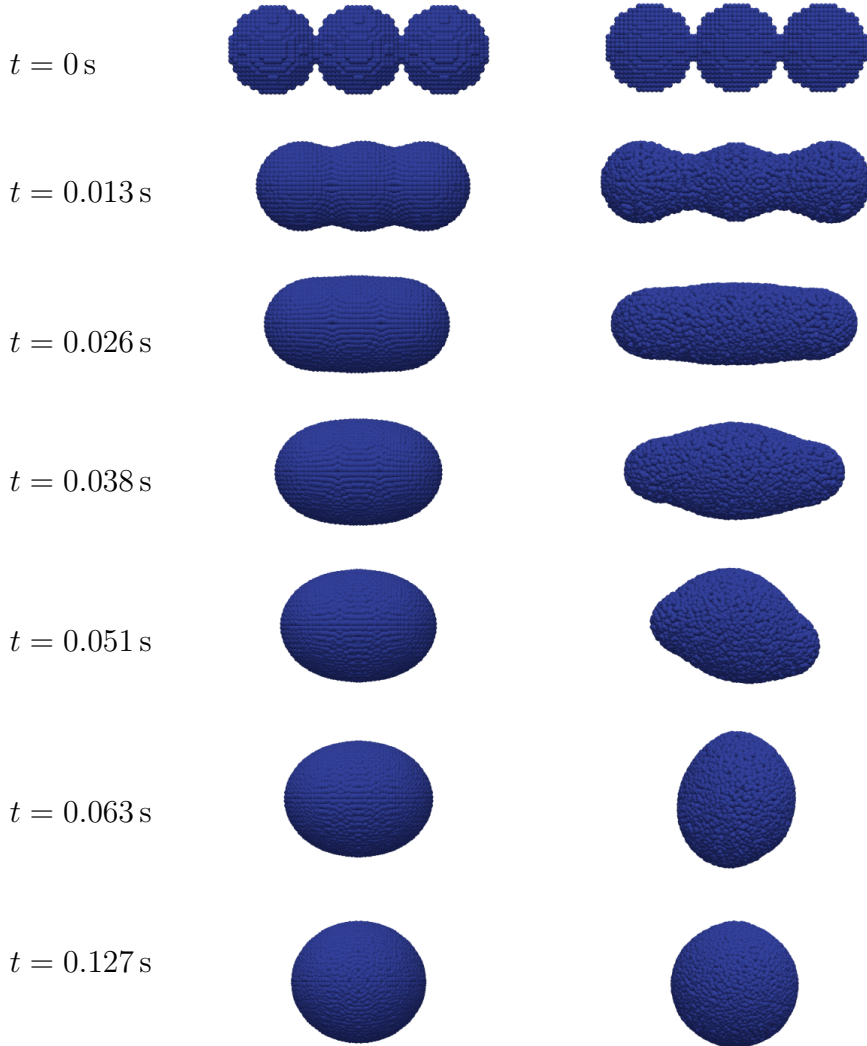


Figure 23: Comparison of the coalescence agglomerates. Left column shows the viscous flow assumption whereas the right column shows the melting process of initially solid particles.

this doesn't span the entire range of properties encountered in real applications. For example, high viscosities encountered in additive manufacturing using polymers would require implicit computation of viscosities. Simulations with high latent heat values require adaptive time stepping to reduce computational costs. These improvements in computational efficiency will enable simulations of large number of particles needed for relating microstructure to bulk properties of manufactured parts.

## Acknowledgements

The authors gratefully acknowledge the support of the Cluster of Excellence Engineering of Advanced Materials, ZISC, FPS and the Collaborative Research Center SFB814 funded by the German Science Foundation (DFG), and the Indo-German Partnership in Higher Education Program (IGP) 2016, funded by DAAD-UGC.

## References

- [1] Adami, S., Hu, X., Adams, N., 2010. A new surface-tension formulation for multi-phase SPH using a reproducing divergence approximation. *J. Comput. Phys.* 229 (13), 5011–5021.
- [2] Beckett, G., Mackenzie, J. A., Robertson, M., 2001. A moving mesh finite element method for the solution of two-dimensional Stefan problems. *J. Comput. Phys.* 168 (2), 500–518.
- [3] Bogner, S., Rüde, U., Harting, J., 2016. Curvature estimation from a volume-of-fluid indicator function for the simulation of surface tension and wetting with a free-surface lattice Boltzmann method. *Phys. Rev. E* 93 (4), 043302.
- [4] Bonacina, C., Comini, G., Fasano, A., Primicerio, M., 1973. Numerical solution of phase-change problems. *Int. J. Heat Mass Transfer* 16 (10), 1825–1832.
- [5] Chen, Q., Guillemot, G., Gandin, C.-A., Bellet, M., 2017. Three-dimensional finite element thermomechanical modeling of additive manufacturing by selective laser melting for ceramic materials. *Addit. Manuf.* 16, 124–137.
- [6] Das, S., 2003. Physical aspects of process control in selective laser sintering of metals. *Adv. Eng. Mater.* 5 (10), 701–711.
- [7] Ehigiamusoe, N. N., Maxutov, S., Lee, Y. C., 2018. Modelling surface tension of two-dimensional droplet using smoothed particle hydrodynamics. *Int. J. Numer. Methods Fluids*.
- [8] Farrokhpahanah, A., Bussmann, M., Mostaghimi, J., 2017. New smoothed particle hydrodynamics (sph) formulation for modeling heat conduction with solidification and melting. *Numer. Heat Transfer, Part B* 71 (4), 299–312.
- [9] Gingold, R. A., Monaghan, J. J., 1977. Smoothed particle hydrodynamics - theory and application to non-spherical stars. *Mon. Not. R. Astron. Soc.* 181, 375–389.
- [10] Guo, N., Leu, M. C., 2013. Additive manufacturing: technology, applications and research needs. *Front. Mech. Eng.* 8 (3), 215–243.
- [11] Gürtler, F.-J., Karg, M., Leitz, K.-H., Schmidt, M., 2013. Simulation of laser beam melting of steel powders using the three-dimensional volume of fluid method. *Physics Procedia* 41, 881–886.
- [12] Hirt, C. W., Nichols, B. D., 1981. Volume of fluid (vof) method for the dynamics of free boundaries. *J. Comput. Phys.* 39 (1), 201–225.
- [13] Hsiao, J., Chung, B. T., 1986. An efficient algorithm for finite element solution to two-dimensional heat transfer with melting and freezing. *J. Heat Transfer* 108 (2), 462–464.
- [14] Hsiao, J.-S., 1983. Numerical and analytical analyses of heat transfer with ablation in a two-dimensional region. Ph.D. thesis, University of Akron.

- [15] Kirchhof, M., Schmid, H.-J., Peukert, W., 2009. Three-dimensional simulation of viscous-flow agglomerate sintering. *Physical Review E* 80 (2), 026319.
- [16] Kreyszig, E., 2010. Advanced engineering mathematics. John Wiley & Sons.
- [17] Lucy, L. B., 1977. A numerical approach to the testing of the fission hypothesis. *Astron. J.* 82, 1013–1024.
- [18] May, D., Monaghan, J., 2003. Can a single bubble sink a ship? *Am. J. Phys.* 71 (9), 842–849.
- [19] McCue, S. W., Wu, B., Hill, J. M., 2008. Classical two-phase Stefan problem for spheres. In: *Proc. R. Soc. London, Ser. A. Vol. 464*. The Royal Society, pp. 2055–2076.
- [20] Mittal, R., Iaccarino, G., 2005. Immersed boundary methods. *Annu. Rev. Fluid Mech.* 37, 239–261.
- [21] Monaghan, J. J., 1992. Smoothed particle hydrodynamics. *Annual review of astronomy and astrophysics* 30, 543–574.
- [22] Morris, J. P., Fox, P. J., Zhu, Y., 1997. Modeling low reynolds number incompressible flows using sph. *J. Comput. Phys.* 136 (1), 214–226.
- [23] Nair, P., Pöschel, T., 2018. Dynamic capillary phenomena using incompressible SPH. *Chem. Eng. Sci.* 176, 192–204.
- [24] Nair, P., Tomar, G., 2014. An improved free surface modeling for incompressible sph. *Comput. Fluids* 102, 304–314.
- [25] Nair, P., Tomar, G., 2015. Volume conservation issues in incompressible smoothed particle hydrodynamics. *J. Comput. Phys.* 297, 689–699.
- [26] Pasandideh-Fard, M., Mostaghimi, J., 1996. Droplet impact and solidification in a thermal spray process: droplet-substrate interaction. *Thermal spray: Practical Solutions for Engineering Problems*, CC Berndt (Ed.), Pub. ASM International, Material Park, Ohio-USA, 637–646.
- [27] Rathjen, K. A., Jiji, L. M., 1971. Heat conduction with melting or freezing in a corner. *J. Heat Transfer* 93 (1), 101–109.
- [28] Riedlbauer, D., Steinmann, P., Mergheim, J., 2014. Thermomechanical finite element simulations of selective electron beam melting processes: performance considerations. *Comput. Mech.* 54 (1), 109–122.
- [29] Rowlinson, J. S., Widom, B., 2013. Molecular theory of capillarity. Courier Corporation.
- [30] Schoinchoritis, B., Chantzis, D., Salonitis, K., 2017. Simulation of metallic powder bed additive manufacturing processes with the finite element method: A critical review. *Proceedings of the Institution of Mechanical Engineers, Part B: Journal of Engineering Manufacture* 231 (1), 96–117.

- [31] Sleijpen, G. L., Van der Vorst, H. A., Fokkema, D. R., 1994. BiCGstab (l) and other hybrid Bi-CG methods. *Numerical Algorithms* 7 (1), 75–109.
- [32] Stewartson, K., Waechter, R., 1976. On Stefan's problem for spheres. In: *Proceedings of the Royal Society of London A: Mathematical, Physical and Engineering Sciences*. Vol. 348. The Royal Society, pp. 415–426.
- [33] Szewc, K., Pozorski, J., Minier, J.-P., 2012. Analysis of the incompressibility constraint in the smoothed particle hydrodynamics method. *Int. J. Numer. Methods Eng.* 92 (4), 343–369.
- [34] Tartakovsky, A. M., Panchenko, A., 2016. Pairwise force smoothed particle hydrodynamics model for multiphase flow: surface tension and contact line dynamics. *J. Comput. Phys.* 305, 1119–1146.
- [35] Thomas, B., Samarasekera, I., Brimacombe, J., 1984. Comparison of numerical modeling techniques for complex, two-dimensional, transient heat-conduction problems. *Metall. Mater. Trans. B* 15 (2), 307–318.
- [36] Voller, V., Cross, M., 1981. Accurate solutions of moving boundary problems using the enthalpy method. *International journal of heat and mass transfer* 24 (3), 545–556.
- [37] Voller, V. R., Prakash, C., 1987. A fixed grid numerical modelling methodology for convection-diffusion mushy region phase-change problems. *Int. J. Heat Mass Transfer* 30 (8), 1709–1719.
- [38] Zhang, M., 2010. Simulation of surface tension in 2D and 3D with smoothed particle hydrodynamics method. *J. Comput. Phys.* 229 (19), 7238–7259.